

High Resolution Tree Height Mapping of the Amazon Forest using Planet NICFI Images and LiDAR-Informed U-Net Model

Fabien H Wagner^{1,2}, Ricardo Dalagnol^{1,2}, Griffin Carter¹,
Mayumi CM Hirye^{1,3,4}, Shivraj Gill¹, Le Bienfaiteur Sagang
Takougoum^{1,3}, Samuel Favrichon^{2,5}, Michael Keller^{2,6}, Jean P.
H. B. Ometto⁸, Lorena Alves^{1,3}, Cynthia Creze^{1,3}, Stephanie
P George-Chacon^{1,3}, Shuang Li¹, Zhihua Liu¹, Adugna
Mullissa^{1,3}, Yan Yang¹, Erone G Santos², Sarah R Worden²,
Martin Brandt^{1,9}, Philippe Ciais^{1,10}, Stephen C. Hagen¹ and
Sassan Saatchi^{1,2,3}

¹ CTrees, Pasadena, CA 91105, US

² Jet Propulsion Laboratory, California Institute of Technology, 4800 Oak Grove,
Pasadena, CA 91109, USA

³ Institute of Environment and Sustainability, University of California, Los Angeles,
CA, USA

⁴ Quapá Lab, Faculty of Architecture and Urbanism, University of São Paulo,
05508080, São Paulo, SP, Brazil

⁵ Gamma Remote Sensing Ag, Gumligen, Switzerland

⁶ USDA Forest Service, International Institute of Tropical Forestry, Rio Piedras,
Puerto Rico, USA

⁷ EMBRAPA Satellite Monitoring, Campinas 13070-115, SP, Brazil

⁸ Remote Sensing Division, National Institute for Space Research—INPE, São José
dos Campos 12227-010, SP, Brazil;

⁹ Department of Geosciences and Natural Resource Management, University of
Copenhagen, Copenhagen, 1350, Denmark

¹⁰ Laboratoire des Sciences du Climat et de l'Environnement, CEA-CNRS-UVSQ,
CE Orme des Merisiers, Gif sur Yvette, 91190, France

E-mail: wagner.h.fabien@gmail.com

22 January 2025

Abstract.

Tree canopy height is one of the most important indicators of forest biomass, productivity, and ecosystem structure, but it is challenging to measure accurately from the ground and from space. Here, we used a U-Net model adapted for regression to map the mean tree canopy height in the Amazon forest from Planet NICFI images at ~ 4.78 m spatial resolution for the period 2020–2024. The U-Net model was trained using canopy height models computed from aerial LiDAR data as a reference, along with their corresponding Planet NICFI images. Predictions of tree heights on the validation sample exhibited a mean error of 3.68 m and showed relatively low systematic bias across the entire range of tree heights present in the Amazon forest. Our model successfully estimated canopy heights up to 40–50 m without much saturation, outperforming existing canopy height products from global models in this region. We determined that the Amazon forest has an average canopy height of ~ 22 m. Events such as logging or deforestation could be detected from changes in tree height, and encouraging results were obtained to monitor the height of regenerating forests. These findings demonstrate the potential for large-scale mapping and monitoring of tree height for old and regenerating Amazon forests using Planet NICFI imagery.

1. Introduction

The Amazon forest is particularly important among the world's forests. It is the most biologically diverse area on the planet, containing around 20% of the diversity of vascular plants, with the number of tree species alone estimated at around 16,000 species (Ter Steege et al., 2013; Zapata-Ríos et al., 2022). In terms of area, the Amazon forest represents > 50% of the world's remaining tropical rainforests, and much of it is still botanically intact (Hansen et al., 2013; Hubbell et al., 2008). The Amazon forest biomass constitutes one of the largest terrestrial carbon pools in the world, estimated at \sim 150 to 200 GtC (Mo et al., 2023; LV et al., 2021). The Amazon forest is still a carbon sink, helping mitigate the effects of global climate change, but the sink is partially offset by disturbances (Pan et al., 2024; Rosan et al., 2024). Recently, the Amazon rainforest has experienced significant changes in tree cover and forest structure due to extensive deforestation (National Institute for Space Research (INPE), Earth Observation General Coordination, 2024; de Almeida et al., 2021), degradation from logging and fire (Matricardi et al., 2020; Lapola et al., 2023; Bourgoin et al., 2024), and increased drought and extreme conditions (Gloor et al., 2013; Marengo and Espinoza, 2016; da Silva et al., 2023). Additionally, some areas of the forest are undergoing regeneration following deforestation; however, our ability to accurately estimate this regrowth and its sink potential is still in its early stages (Heinrich et al., 2021; Silva Junior et al., 2020; Heinrich et al., 2023; Bastin et al., 2019; Mo et al., 2023). To protect the carbon sink and biodiversity, make policies to limit deforestation, improve timber-harvesting practices, and identify potential areas for forest restoration (Pan et al., 2024; Mo et al., 2023), a better estimation of forest structure and biomass, as close as possible to the level of individual trees, is needed. While both values can be derived from canopy height (Asner and Mascaro, 2014; Lim et al., 2003; Longo et al., 2016), which is also recognized as an Essential Biodiversity Variable (EBV) on the priority list of biodiversity metrics to observe from space (Skidmore et al., 2021), estimating canopy height at the domain scale remains a challenging task for remote sensing techniques.

To estimate forest canopy height, airborne LiDAR (Light Detection and Ranging) is the gold standard; however, data acquisition is limited to sparse, local to regional-scale coverage due to the high costs associated with it. Notably, in the Brazilian Amazon, significant efforts have been made to flight airborne LiDAR to capture the diversity of forest structure using a scientifically-based sampling design and over permanent plots in the Amazon forest where field studies are conducted (Ometto et al., 2023; Dos-Santos et al., 2022). A secondary dataset used to estimate forest structure and tree height is the Global Ecosystem Dynamics Investigation (GEDI) mission data (Dubayah et al., 2020). While of utmost importance for the scientific community, these data are sparse and represent only a few percent of the entire Amazon forest domain. To estimate tree height on a larger scale than LiDAR flight lines or GEDI point height measurements, a novel approach is to train machine/deep learning models with common multispectral

and/or radar remote-sensed images to estimate reference heights measured from LiDAR or GEDI data. These models can then be applied to regions, countries, or even globally, where reference canopy height data are not available. For example, estimations of tree height have already been made using Landsat images (Potapov et al., 2021), Sentinel-2 images (Lang et al., 2019, 2023; Astola et al., 2021), combinations of Sentinel-1 (radar) and Sentinel-2 (multispectral) (Ge et al., 2022; Fayad et al., 2023; Schwartz et al., 2023, 2024; Pauls et al., 2024), Planet images (Liu et al., 2023; Csillik et al., 2019; Huang et al., 2022), and very high-resolution images from airborne sources (Wagner et al., 2024; Li et al., 2023, 2020; Karatsiolis et al., 2021) and Maxar satellite data (Illarionova et al., 2022; Tolan et al., 2024).

Most global models using canopy height use open datasets such as Landsat or Sentinel-1 and -2 (Potapov et al., 2021; Lang et al., 2023; Pauls et al., 2024). However, these datasets are currently not ideal for the Amazon due to their temporal resolution, which is insufficient for frequent cloud-free data, their spatial resolution of 30 or 10 meters, which is too coarse to identify individual trees, and the incomplete coverage of the Amazon (Sentinel-1). Another dataset currently used by Meta is the Maxar Vivid2 mosaic imagery (Tolan et al., 2024). However, this data still contains clouds and, as a result, remains incomplete for the Amazon forest.

The best current open data for the Amazon forest and the tropics are the Planet satellite images provided by Norway's International Climate and Forest Initiative (NICFI, <https://www.nicfi.no/>) (Planet Team, 2017). The Planet NICFI images are multispectral, including red, green, blue, and near-infrared bands, with a spatial resolution of 4.78 meters for the Normalized Analytic Basemaps. They cover tropical forest regions between 30 degrees North and 30 degrees South. The temporal resolution of the NICFI images is one month, and each image is a mosaic composite of the best daily acquisitions within that month. Consequently, Planet NICFI images are mostly cloud-free, providing the best freely available multispectral dataset to monitor Land Use and Land Cover (LULC) changes in tropical regions. The absolute radiometric accuracy is not guaranteed for the normalized surface reflectance basemaps (Pooja Pandey and Curdoglo., 2021), which limits the use of traditional pixel-based machine learning methods. However, this does not impede the extraction of accurate information using deep learning methods, which rely more on pixel context and multiple levels of abstraction (LeCun et al., 2015). For example, it has been shown that with a deep learning model such as the U-Net model (Ronneberger et al., 2015), tree cover (Wagner et al., 2023) or degradation from logging, fire, or roads (Dalagnol et al., 2023) can be accurately mapped in the tropics using Planet NICFI images (CTrees.org, 2024).

Examples of regional or larger-scale tree height vegetation mapping with deep learning are rare in the tropics and typically come from global datasets (Lang et al., 2023; Tolan et al., 2024; Pauls et al., 2024), while such methods are slightly more developed in other regions, such as boreal and temperate forests (Astola et al., 2021; Fayad et al., 2023; Schwartz et al., 2023, 2024; Liu et al., 2023; Wagner et al., 2024; Li et al., 2023; Illarionova et al., 2022). With the exception of Tolan's model (Tolan et al.,

2024), which uses a fine-tuned foundation model – a completely different type of deep learning approach requiring multiple high-end GPUs – most other studies demonstrate that tree height estimation can be achieved with great accuracy using encoder-decoder deep learning architectures trained locally, such as U-Net (Ronneberger et al., 2015).

Here, we present a U-Net deep learning model adapted for regression which can directly predict tropical vegetation height from Planet NICFI images. It was trained using canopy height model (CHM) data from the Brazilian Agricultural Research Corporation (Embrapa), the National Institute for Space Research (INPE, Brazil), and the São Paulo City Hall (Brazil), and their corresponding Planet NICFI images. The model exclusively estimates vegetation height and differentiates it from other objects with height in LiDAR canopy height models, like buildings. The validation with LiDAR datasets sampled across the Amazon is presented. Our canopy height estimates were compared to the available medium and very high-resolution global canopy height models from Sentinel-2 and -1 (10 m) and Maxar Vivid2 mosaic imagery (0.5 m). We also show the evolution of tree height after events such as deforestation, logging, and regeneration. Finally, the Amazon forest tree height map at 4.78 m of spatial resolution for the year 2020 is provided.

2. Methods

2.1. *Planet NICFI satellite images*

To train the model and predict the tree canopy height of the Amazon forest, we used Planet satellite images over the tropics made available by Norway's International Climate and Forest Initiative (NICFI, <https://www.nicfi.no/>) (Planet Team, 2017). The Planet tiles of $\sim 20 \times 20$ km at approximately 4.78 m spatial resolution covering the LiDAR flight lines and the entire Amazon region (approximately 8,260,920 km², 22,047 quads per basemap) were downloaded through the Planet API <https://api.planet.com/basemaps/v1/mosaics> and with the PlanetNICFI R package (Mouselimis, 2022) for all 56 available dates (Planet Team, 2017) at the time of the study (2024-06-01 included). The complete dataset contained approximately 1,240,000 Planet images with a biannual temporal resolution from 2015-12-01 to 2020-06-01 and a monthly temporal resolution from 2020-09-01 to 2024-06-01. All bands in raw image digital numbers (12 bits), Red (0.650-0.682 μm), Green (0.547-0.585 μm), Blue (0.464-0.517 μm), and the NIR bands (0.846-0.888 μm) (Planet, 2021), were first truncated to the range 0–2540 for the RGB bands and scaled between 0 and 2540 for the NIR bands (i.e., divided by 3.937). Second, the 4 bands were scaled to 0–255 (8 bits) by dividing by 10, and then the Red-Green-Blue-NIR (RGBNIR) composite was built. The forest reflectance values are low in the RGB bands (< 500), and the specific scaling of these bands was made to optimize the range of values of the forest reflectance in 8 bits. The scaling of NIR is only a min-max (0-10000) scaling as forest reflectance values are not low in this band. No atmospheric correction was performed.

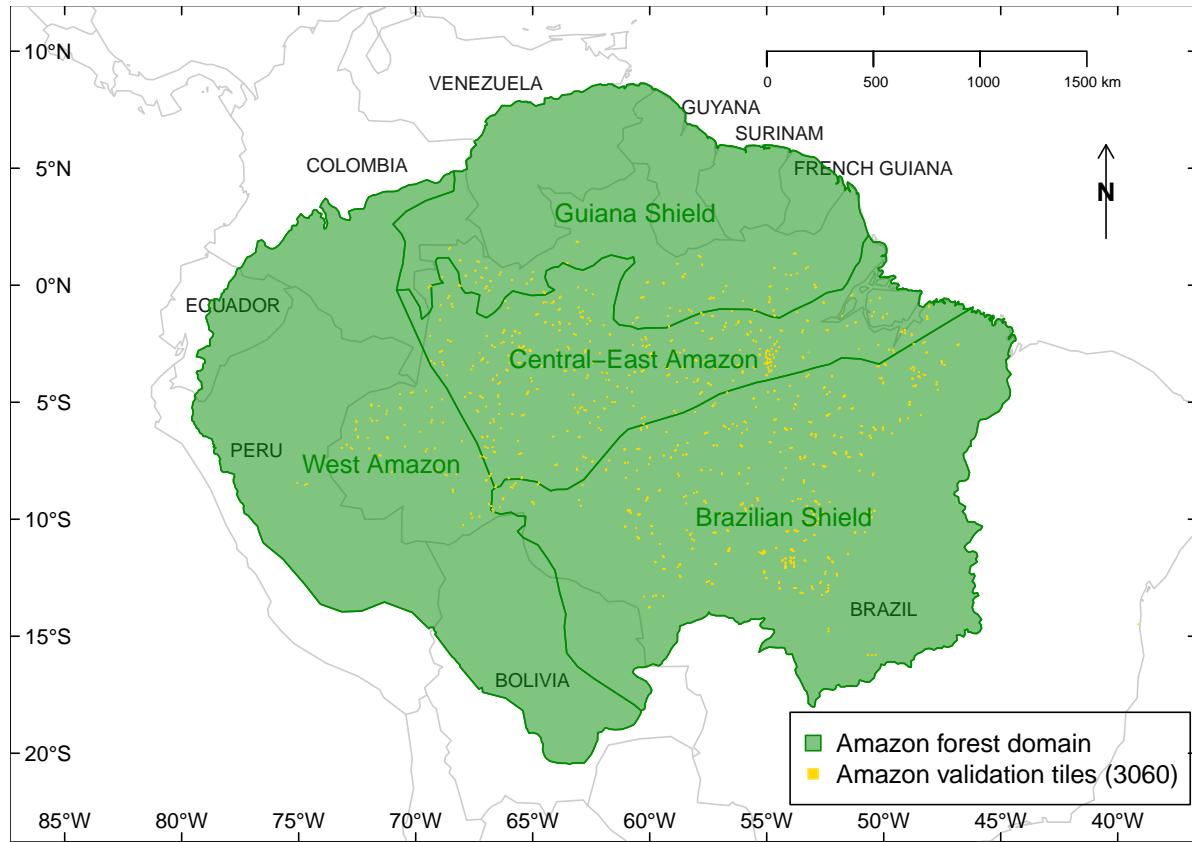


Figure 1. Location of the 3,060 LiDAR data points in the Amazon domain used in the validation of the Amazon forest tree canopy height model (shown in gold). As at least one image per flight was used in validation, the validation locations approximately represent the locations of all the LiDAR flights in the Amazon used in the study. The Amazon domain is partitioned into four regions according to Feldpausch et al. (2011).

2.2. LiDAR dataset

The LiDAR datasets to train the model were obtained from the Brazilian Agricultural Research Corporation (Embrapa), the National Institute for Space Research (INPE, Brazil), and the São Paulo City Hall (Brazil).

The Embrapa datasets were collected for the "Sustainable Landscapes - Brazil" Program, which aims to quantify carbon stocks and assess the impact of human activity on changes in carbon stocks in the Amazon Forest (Dos-Santos et al., 2022). The project was part of the "Sustainable Landscapes" program of technical cooperation from USAID and the U.S. Department of State, with operations in more than 40 countries. In Brazil, the program was related to improving carbon accounting and greenhouse gas emissions, focusing on the transfer of technologies and advanced training programs for professionals working in research and management of natural resources, mainly forest resources. In this regard, LiDAR data were acquired from airborne surveys in the Amazon, Cerrado, and Atlantic forest domains during the period from 2008 to 2018

(https://daac.ornl.gov/CMS/guides/LiDAR_Forest_Inventory_Brazil.html and <https://www.paisagenslidar.cnptia.embrapa.br/>). The project is still ongoing and continues to collect LiDAR flights to this date (06/05/2024). The dataset is publicly available and distributed in LAZ files. The spatial resolution required by the program was approximately 10 points per m², distributed in 1 km² tiles over key field research sites. From the Embrapa dataset, we used all LiDAR datasets (23 sites) from 2015, 2016, 2017, and 2018 in Brazil, and one dataset from 2017 in Peru (1 site), which represents 1,149 LAZ files.

The EBA (Biomass Estimation of the Amazon) project LiDAR transects across the Brazilian Amazon were collected during two campaigns (2016/2017 and 2017/2018) (Ometto et al., 2023). Data and metadata were downloaded from <https://zenodo.org/records/7636454> and <https://zenodo.org/records/4968706>. Some transects were randomly distributed over the forest and secondary forest, some were randomly distributed over the deforestation arch, and others overlapped field plots to allow for model calibration. Each transect covered a minimum of 375 hectares (12.5 km × 300 m) and was surveyed by emitting full-waveform laser pulses from a Trimble Harrier 68i airborne sensor (Trimble; Sunnyvale, CA) aboard a Cessna aircraft (model 206). The average point density was set at four returns per m², the field of view was 30°, the flying altitude was 600 m, and the transect width on the ground was approximately 494 m. Global Navigation Satellite System (GNSS) data were collected on a dual-frequency receiver (L1/L2). The pulse footprint was below 30 cm, based on a divergence angle between 0.1 and 0.3 milliradians. Horizontal and vertical accuracy were controlled to be under 1 m and 0.5 m, respectively. From this dataset, we used 19,302 LAZ files of a maximum size of approximately 1000 × 1000 m.

The LiDAR dataset covering the São Paulo Metropolitan Region (SPMR) was acquired in aerial campaigns conducted in 2017. The dataset is publicly available and distributed in LAZ files at <https://registry.opendata.aws/pmsp-lidar/>. This dataset was used to help the model learn a more diverse background (pasture, exposed soil, building) and to have some data for the Atlantic forest to help the model generalize. The LiDAR survey was conducted from February to June 2017 with the Optech Gemini airborne sensor aboard a helicopter with the following characteristics: Frequency 100-125 KHz; scan angle 18-25 degrees; beam divergence 0.25 mrad; average flight height 700 m; and average nominal density of 8 returns per m². From this dataset, we used 5,554 LAZ files of approximately 500 × 500 m.

Canopy height models (CHM) were generated for all the point clouds (originally in .LAZ file format) using the `LidR` R package (Roussel et al., 2020; Roussel and Auty, 2021). First, the LiDAR point clouds were denoised to remove outliers using the `ivf` algorithm with parameters of 1 m for resolution and 5 for the maximal number of other points in the surroundings (Roussel and Auty, 2021). Second, the point cloud was classified using the `pmf` algorithm with parameters `ws = seq(4, 42, 3)`, or `ws = seq(3, 12, 3)` if the algorithm had difficulty converging, and `th = seq(0.1, 1.5, length.out = length(ws))`. Third, the digital terrain model (DTM) and the digital surface model

(DSM) were computed at 1 m spatial resolution using the *TIN* algorithm (Roussel and Auty, 2021) and the *pitfree* algorithm (thresholds of [0,2,5,10,15] and maximum edge length of [0, 1.5]), respectively. Fourth, the CHM was computed as the difference between DSM and DTM, multiplied by a factor of 2.5, and saved in integer 8 bits. The scaling enables us to maximize the resolution for height data in integers while staying within the limits of the 8-bit integer system, where 255 is the maximum value.

2.3. Building footprints masking

The Building Footprints datasets of South America made by Google (<https://sites.research.google/open-buildings/>) were used to mask the heights of buildings that often appear erroneously in the CHM. A buffer was added to the polygons of buildings, and the buffered polygons were rasterized to the CHM resolution. The buffer had values of 5 m outside cities and 15 m inside cities. The values of the buffer were selected as a compromise between eliminating all house and building pixels, even in the presence of a geolocation error between the CHM and the building footprints dataset, and avoiding the masking of nearby trees. All CHM pixels overlapped by the buffered building footprints were set to zero.

2.4. Global tree height datasets

The results of the model were compared to three recent global height datasets for our 3,436 validation images of size 256×256 pixels. The first height dataset is taken from a global canopy height map for the year 2020 developed by Meta and based on Tolan's model (Meta and World Resources Institute (WRI), 2023; Tolan et al., 2024). This height map was produced at a 0.5 m spatial resolution using the self-supervised DINOv2 model and a machine learning approach to estimate CHM from Maxar RGB satellite imagery, with aerial and GEDI LiDAR used as reference data for model training (Meta and World Resources Institute (WRI), 2023). The second height dataset was obtained from a global CHM for the year 2020, Lang's model (Lang et al., 2023). This height map was generated at a 10 m spatial resolution using CNN and Sentinel-2 reflectance data, also referencing GEDI LiDAR data for vegetation height. Currently, this dataset represents the most accurate freely available global vegetation height dataset. The third height dataset was obtained from a global CHM for the year 2020, Pauls's model (Pauls et al., 2024). This height map was generated at a 10 m spatial resolution using CNN, Sentinel-2 reflectance data and Sentinel-1 and also using GEDI LiDAR data as the reference for vegetation height .

2.5. Deforestation and logging datasets

To analyze changes in tree canopy height in areas of deforestation and logging, we used two datasets based on Planet NICFI images to locate regions of interest and date the events. The deforestation dataset provides the month when deforestation occurs

in pan-tropical evergreen forests (Wagner et al., 2023; CTrees.org, 2024). The logging dataset provides the areas of logging every 6 months in the pan-tropical evergreen forests (Dalagnol et al., 2023; CTrees.org, 2024).

2.6. Neural Network Architecture

The canopy height estimation from the Planet NICFI images of the Amazon forest was performed using a classical U-Net model (Ronneberger et al., 2015) with approximately 35 million parameters, as depicted in Fig. 2. Specifically, the U-Net model predicted the canopy height for each pixel of the input image. The model input was a 4-band RGB-NIR image with dimensions of 256×256 pixels and a spatial resolution of 4.78 m. The output of the model was a single-band image with dimensions of 256×256 pixels, containing values ranging from 0 to 1 (representing 0 to 100 m when unscaled). The model was implemented using the R language (R Core Team, 2016) with the RStudio interface to Keras and TensorFlow 2.10 (Chollet et al., 2015; Allaire and Chollet, 2016; Allaire and Tang, 2020; Abadi et al., 2015).

2.7. Training and validation

To generate samples for model training and validation, we initially selected all Planet NICFI images that overlapped with the CHM and had the closest date to the corresponding LiDAR flight. To increase the sample size and mitigate the effects of cloud contamination, we also included Planet NICFI images from the previous and subsequent dates, assuming no significant change in forest height occurred within a time window of up to one year. This corresponds to ± 6 months for biannual Planet NICFI time series and ± 1 month for monthly Planet NICFI time series.

Subsequently, we resampled the 1 m spatial resolution CHM rasters into an empty raster of one band with the extent and resolution (4.78 m) of the corresponding Planet NICFI image using the median function. Additionally, we resampled a binary raster indicating presence/absence of CHM data at 1 m spatial resolution into an empty raster of one band with the extent and resolution (4.78 m) of the corresponding Planet NICFI image using the minimum function. Since some flights do not cover the entire 256×256 pixel image, this additional dataset of CHM data presence/absence is used later to weight the model's loss function.

In the third step, the Planet NICFI images and corresponding resampled CHM, as well as the binary CHM presence/absence rasters, originally sized at 4096×4096 pixels, were divided into image patches of 256×256 pixels using the `gdal_retile` tool (GDAL/OGR contributors, 2019).

The final sample comprised a total of 50,724 256×256 -pixel image patches, each containing 4 bands, with an associated single-band CHM image and a single-band CHM binary presence/absence map. Of these, 47,288 images were used for training, and 3,436 (7.2%) for validation. Within the validation sample, 3,060 images were distributed across the Amazon forest domain and 376 across the Brazilian Atlantic forest domain. We

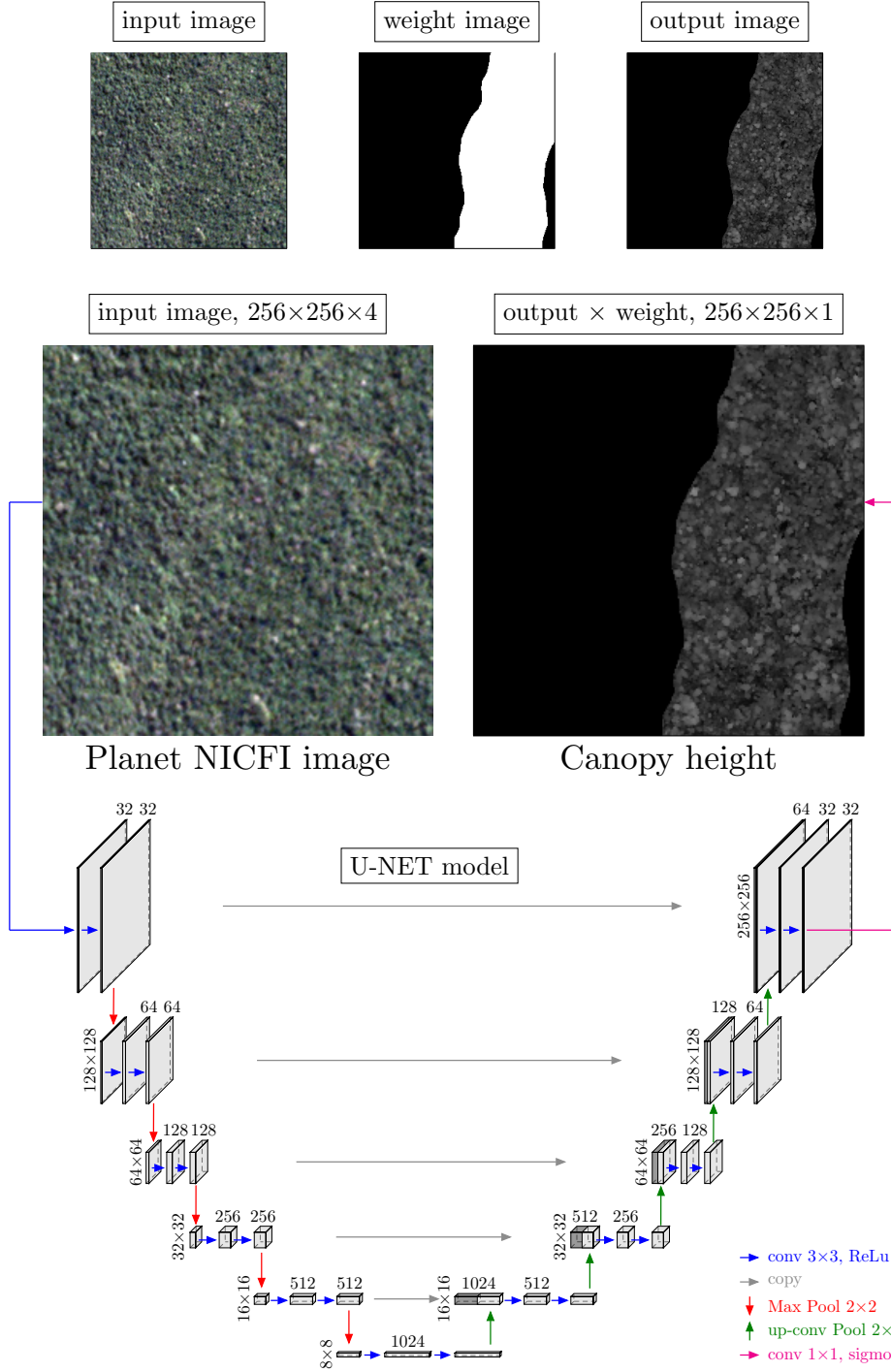


Figure 2. U-Net model architecture used for canopy height estimation from Planet NICFI images, adapted from Ronneberger et al. (2015). The number of channels is indicated above the cuboids, and the vertical numbers indicate the row and column sizes in pixels. The operations (convolutions, skip connections, max pooling, and upsampling) performed in each layer and their sizes are indicated by the colored arrows.

created a spatially uniform validation sample by selecting one image from each NICFI tile extent covering the CHM dataset. This approach aimed to capture the diverse

vertical structures of the Amazon forest.

The absolute radiometric accuracy is not guaranteed for the normalized surface reflectance NICFI basemaps (Pooja Pandey and Curdoglo., 2021). Consequently, the variation of reflectance values between different Planet satellite sensors, between dates, and sometimes within the same image is high. Therefore, no data augmentation was applied during training.

During the network training, we used standard stochastic gradient descent (SGD) optimization and the Adam optimizer (learning rate of 0.0001). SGD optimization was used to minimize the loss function by using random mini-batches of data, allowing for faster convergence and improved generalization (Chollet and Allaire, 2018). Mean squared error was used as the loss function, and mean absolute error as the accuracy metric. The loss function was weighted by the binary presence/absence of CHM data. The network was trained for 1,000 epochs with a batch size of 32 images. These parameters allowed us to achieve the highest accuracy within a reasonable time frame, as observed in a previous model run. The model with the best validation accuracy (i.e., validation loss of 0.0008285521 and a mean absolute error of 3.62) was kept for prediction. The training of the models took less than a day using an Nvidia RTX4090 Graphics Processing Unit (GPU) with 24 GB of memory.

2.8. Amazon Forest 2020-2024 Canopy Height Map

For prediction, NICFI tiles were resized by adding columns and rows filled with mirrored images, resulting in 4224×4224 -pixel images corresponding to the original 4096×4096 size with a 64-pixel border. Predictions were made on these 4224×4224 -pixel images, and the 64-pixel border of each prediction was removed to mitigate border artifacts (Ronneberger et al., 2015). The mean height of the Amazon forest for the period 2020–2024 was computed as the average of all observed heights for each pixel during the period from January 1, 2016, to June 1, 2024, excluding pixels with clouds or shade, deforested areas before 2020, and regenerated areas after 2020. We assume that there was no significant height change due to growth between 2020 and 2024. We also kept the number of non-cloud observations per pixel as a confidence index. For the forested pixels (height above 5 m), we computed the mean canopy height using the mean height per tiles and number of valid observation of tree height per tiles as weight, eqn 1, were i is a planet quad and valid observation is a pixel with tree height above 5 m and number of non-cloud observation above 5. The weighted percentile 2.5, 5, 25, 50, 75, 95 and 97.5 over the Amazon were also computed using the same per-tile logic.

$$\text{weighted mean} = \frac{\sum_{i=1}^n (\text{mean}_i \times \text{valid observations}_i)}{\sum_{i=1}^n \text{valid observations}_i} \quad (1)$$

3. Results

3.1. Accuracy and comparison with global CHM models

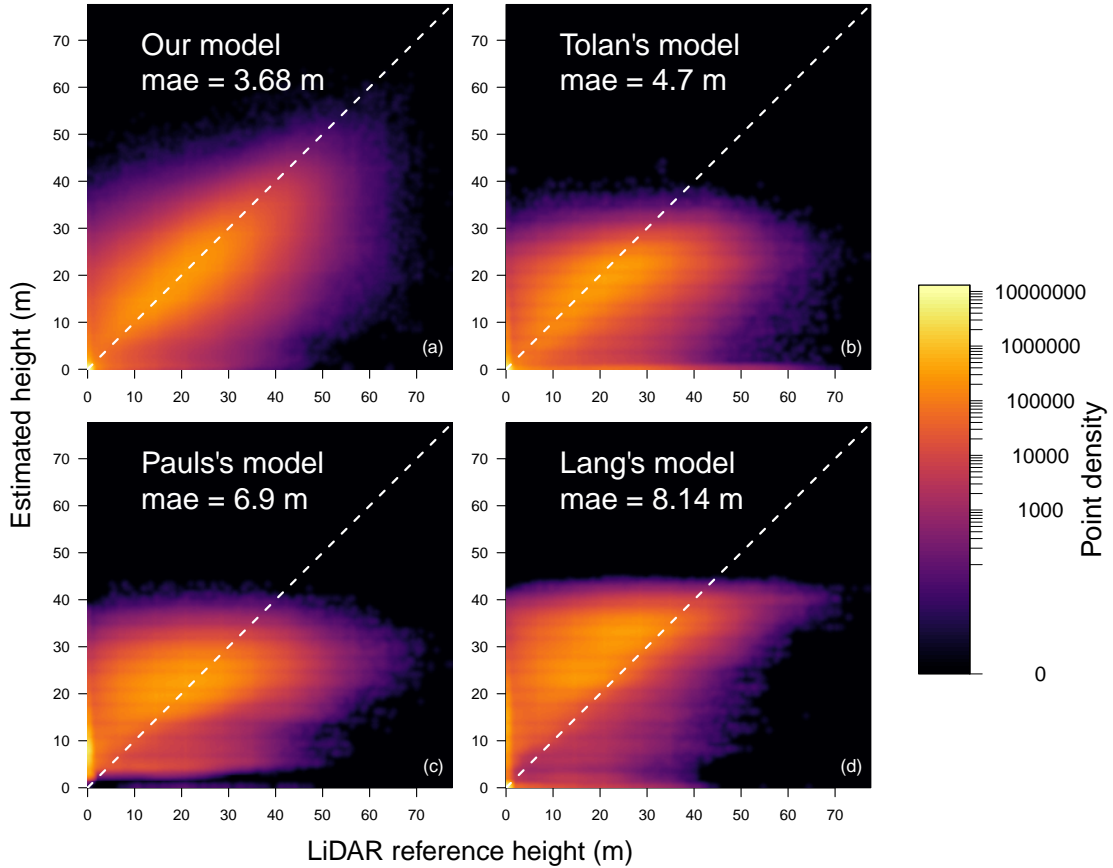


Figure 3. Comparison of predicted versus observed height (m) for the 3,436 validation areas represented as density scatterplots for our canopy height model (a), Tolan's model (b), and Lang's model (c). Tolan's model and Lang's model, with native spatial resolutions of 0.5 m and 10 m respectively, were warped to our 4.78 m spatial resolution using the median and nearest neighbor algorithms, respectively. Each plot contains approximately 63 million points. The 1:1 line and the mean absolute error are depicted in white.

Our model accurately predicted tree canopy height, as evidenced by the alignment of predictions and observations along the 1:1 line for most of the 3,436 validation areas, Fig. 3a. The mean absolute error was 3.68 m. The model can reach heights up to 45–50 m and, in a few cases, even higher but underestimated all trees above 50 m. However, in the validation data, pixels above 50 m represent only 37,318 pixels, which is 0.06% of the pixels in the validation. Our model seems to work well for the non-forest height, as seen by the high density near zero, Fig. 3a. For canopy heights below 25 m, the model tends to slightly overestimate the height. It is important to note that the Planet and CHM images are not co-registered, and, as the Planet NICFI basemap is a mosaic

made of the best daily images over one month, one NICFI image can contain images at different dates and with different sensor calibrations.

In comparison, Tolan's canopy height model based on Maxar data at 0.5 m spatial resolution for the year 2020 (Tolan et al., 2024) only reaches canopy heights up to 30-35 m and shows a significant saturation effect, as shown in Fig. 3b. The mean absolute error of Tolan's canopy height model is 4.7 m on the validation dataset. Many pixels are also predicted to have zero height, mainly due to the presence of clouds in their dataset, as indicated by the high density near zero for predicted heights compared to observed heights, as seen in Fig. 3b. Similar to our model, they also tend to overestimate canopy heights below 25 m.

Pauls's canopy height model based on Sentinel-2 and Sentinel-1 data at 10 m spatial resolution for the year 2020 (Pauls et al., 2024) shows a similar saturation effect to the Tolan's model and cannot reach canopy heights above 40 m, as shown in Fig. 3c. The mean absolute error of Pauls's canopy height model is 6.9 m on the validation dataset. Pauls's model also tends to overestimate non-forest and low vegetation canopy height. Predicted height values start strictly above 2-3 m.

Lang's canopy height model based on Sentinel-2 data at 10 m spatial resolution for the year 2020 (Lang et al., 2023) can reach canopy heights up to 40-45 m, as shown in Fig. 3d. The mean absolute error of Lang's canopy height model is 8.14 m on the validation dataset. Although Lang's model tends to overestimate canopy height, which is expected due to the 10 m spatial resolution, it effectively captures tall trees.

3.2. Predicted height distribution analysis

The distribution of observed heights in the validation sample shows a bimodal pattern with a sharp peak at zero and another centered around 20 m, Fig. 4a. Our model exhibits a distribution similar to the observed heights and tends to predict heights more uniformly across the entire range compared to Tolan's, Pauls's or Lang's models, Fig. 4b. The peak around 20 m in our model is slightly lower than observed, likely due to slight underestimation above 20 m and slight overestimation below 20 m, while the peak at zero is similar to the observed distribution.

Tolan's model displays a narrower distribution with a prominent peak around 20 meters, reflecting underestimation of heights above 20 m. Additionally, Tolan's model shows a higher peak near zero, indicating more instances of zero height than observed, likely due to cloud cover in the Maxar images.

Pauls's model displays a two-peaks distribution with a higher peak around 22-23 m, Fig. 4b, reflecting an overestimation of the canopy height. Additionally, Pauls's model shows a second peak between 5 and 10 m and no values near zero, indicating height overestimation of non-forest and low vegetation pixels.

Lang's model, Fig. 4b, tends to overestimate heights and exhibits a distribution with three peaks: a peak near zero lower than expected, and two peaks around approximately 24 m and 33 m that are higher than expected.

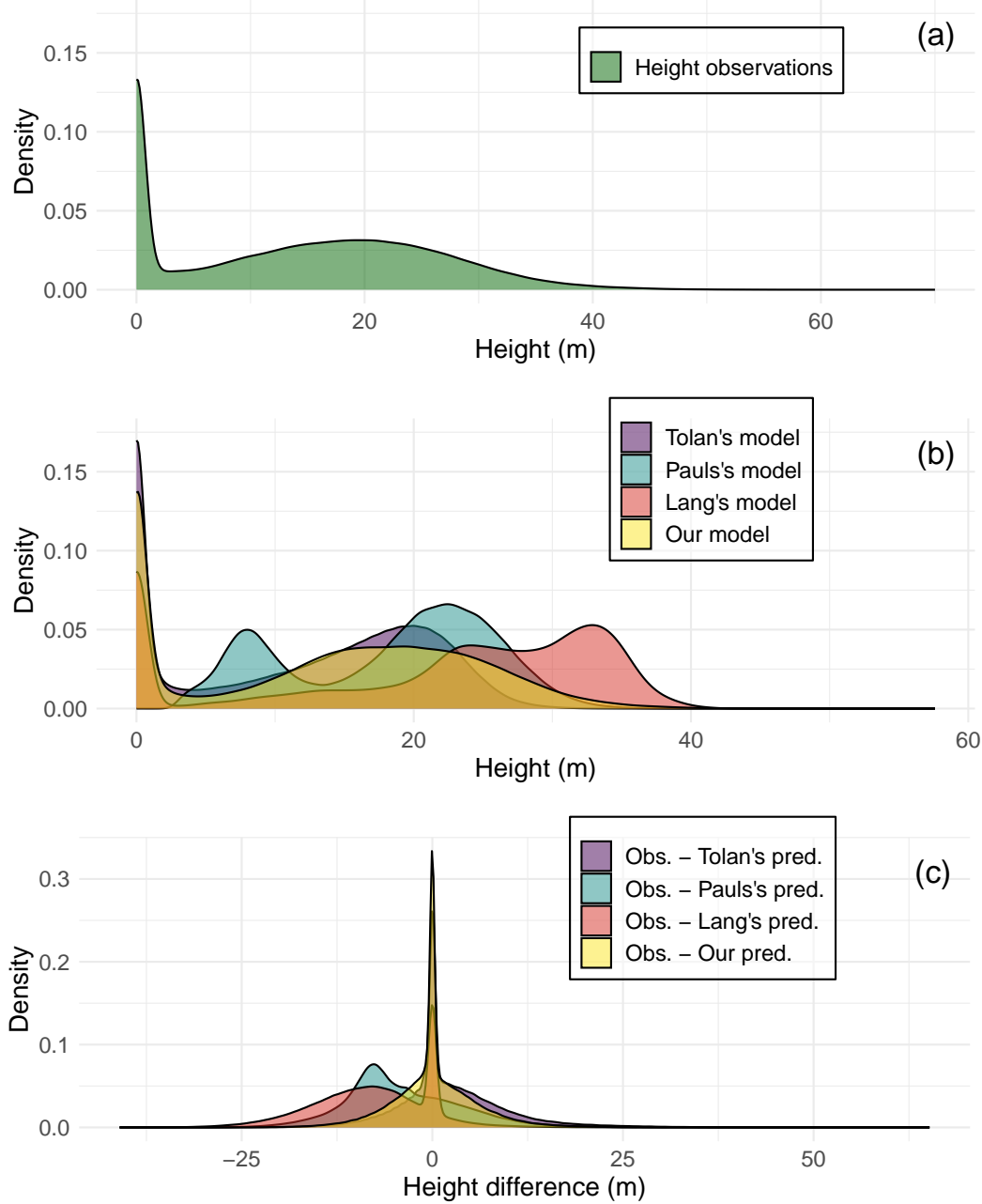


Figure 4. Distribution of the observed height in the validation sample (a); distribution of the predicted height in the validation sample for our model, Tolan's model, and Lang's model (b); and distribution of the differences in predicted height in the validation sample between our model and Tolan's model, and between our model and Lang's model (c), respectively.

The height differences between predicted heights from our model, Tolan's model, and Lang's model are centered around zero, with peak values of 0.33, 0.27, and 0.15, respectively (Fig. 4c), suggesting that the models, to a certain extent, can predict the observed heights, with our model outperforming the other two. On the other hand,

Pauls's model shows a unimodal distribution with a single peak in the negative height differences, indicating an overall tendency to overestimate heights. The distribution of differences for our model is more uniformly distributed around zero, while Tolan's model exhibits an excess of positive differences and a lack of negative differences, likely due to overall underestimation of heights above 20-30 m. Similarly to Pauls's, Lang's model exhibits a broader distribution of negative height differences, suggesting the same overestimation tendency.

3.3. Example of predictions from the models

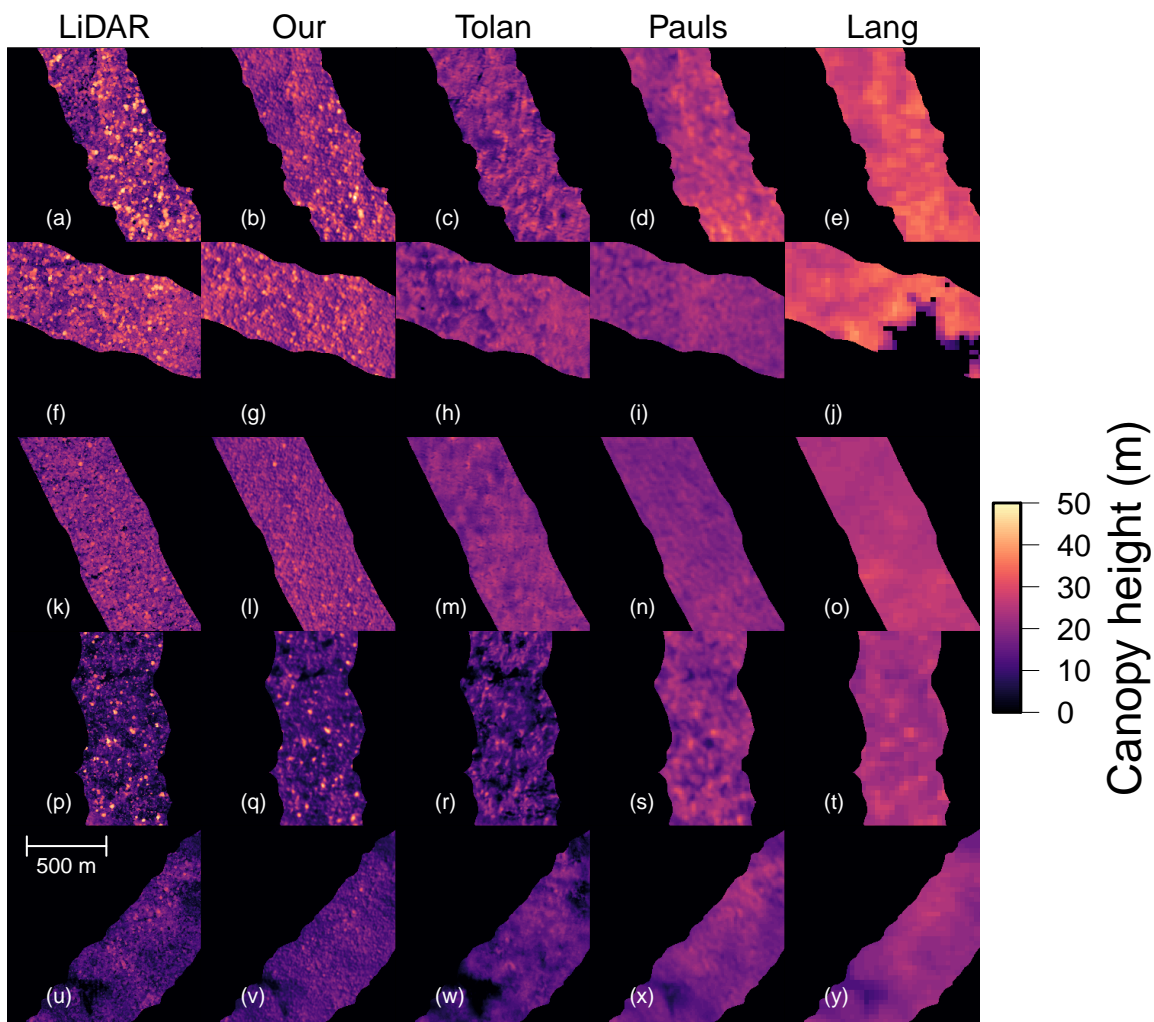


Figure 5. Example of canopy height models observed in the validation dataset (column 1), predicted from our canopy height model (column 2), predicted from Tolan's model (column 3), and predicted from Lang's model (column 4). Tolan's model, Pauls's model and Lang's model, whose native spatial resolutions are 0.5 m, 10 m and 10 m, respectively, have been warped to our 4.78 m spatial resolution using the median and nearest neighbor algorithms, respectively.

Our model can reproduce the CHM up to the crown level in different forest structure

configurations, Fig. 5. In dense forests with tall trees, Fig. 5a-e, although heights may be underestimated, the crowns are clearly identifiable in both the reference and our model, Fig. 5a and b. In Tolan's model, Fig. 5c, while some crowns are identifiable, the CHM appears more blurry. Furthermore, Tolan's model seems to capture lower points of the CHM compared to our model. In Pauls's model, Fig. 5d, some high and large crowns of the reference dataset are visible, and the CHM appears better than Tolan's model for those tall trees, but the model struggles for lower points. Lang's model, Fig. 5e, can identify groups of trees and appears to closely follow the overall height pattern of the tallest points in the canopy.

For dense forests with less variation in the canopy, Fig. 5f-j, our model (Fig. 5g) still captures crowns, while Tolan's model (Fig. 5h) rarely reaches the crown levels, except for large trees. Pauls's model (Fig. 5i) also captures some crowns but overall underestimates the height of taller trees. In Lang's model for this image, there is missing data likely due to clouds (Fig. 5j).

For lower-density forests, Fig. 5k-o, our model still captures the crowns but misses the lower points and gaps in the canopy, Fig. 5l. For this type of forest, Tolan's model is blurry and does not reach crown levels, except for some very large tall trees, Fig. 5m. Pauls's canopy height is closer to our results but appears more blurry, Fig. 5n. In Lang's model, Fig. 5o, similar to Fig. 5e, it appears to follow the overall height and structure of the highest points in the canopy.

For low forests with isolated large tree crowns, Fig. 5p-t, our model captures the crowns well and also predicts the height well for large gaps in the canopy, Fig. 5q. For this type of forest, Tolan's model, Fig. 5r, predicts some of the largest crowns and seems to predict the gaps and lower points of the CHM very well. Pauls's model overestimates the lowest canopy heights but seems to predict some of the largest crowns, Fig. 5s. In this area, Lang's model, Fig. 5t, is able to capture very tall heights of small groups of trees, but overall shows a tendency to overestimate canopy height.

For the low forest with minimal variation in structure, Fig. 5u-y, our model still offers the best resolution for the CHM data, Fig. 5v, but it may miss some of the lower points that Tolan's model can reach, Fig. 5w. Pauls's model overestimates most canopy heights and low areas of the forest, and only some large individual crowns are visible, Fig. 5x. While showing some overestimation, Lang's model (Fig. 5y) captures the overall spatial pattern of canopy height.

For forests with a smooth transition to very low canopy heights, Fig. 6a-e, our model (Fig. 5b) still offers good resolution for the CHM data and is able to reach low heights, similar to what Tolan's model can achieve, Fig. 5c. The pattern of smooth changes in canopy height is also present in Pauls's and Lang's models (Fig. 5d-e), but both show canopy height overestimation.

For rivers inside the forest (Fig. 6f-j), our model is able to map water bodies with a height of zero, Fig. 5g, similar to Tolan's model (Fig. 5h). In Pauls's model only larger portion of the river appeared, Fig. 5i. In Lang's model, Fig. 5j, some rivers appear higher than the surrounding forest, possibly due to shading effects on the river border

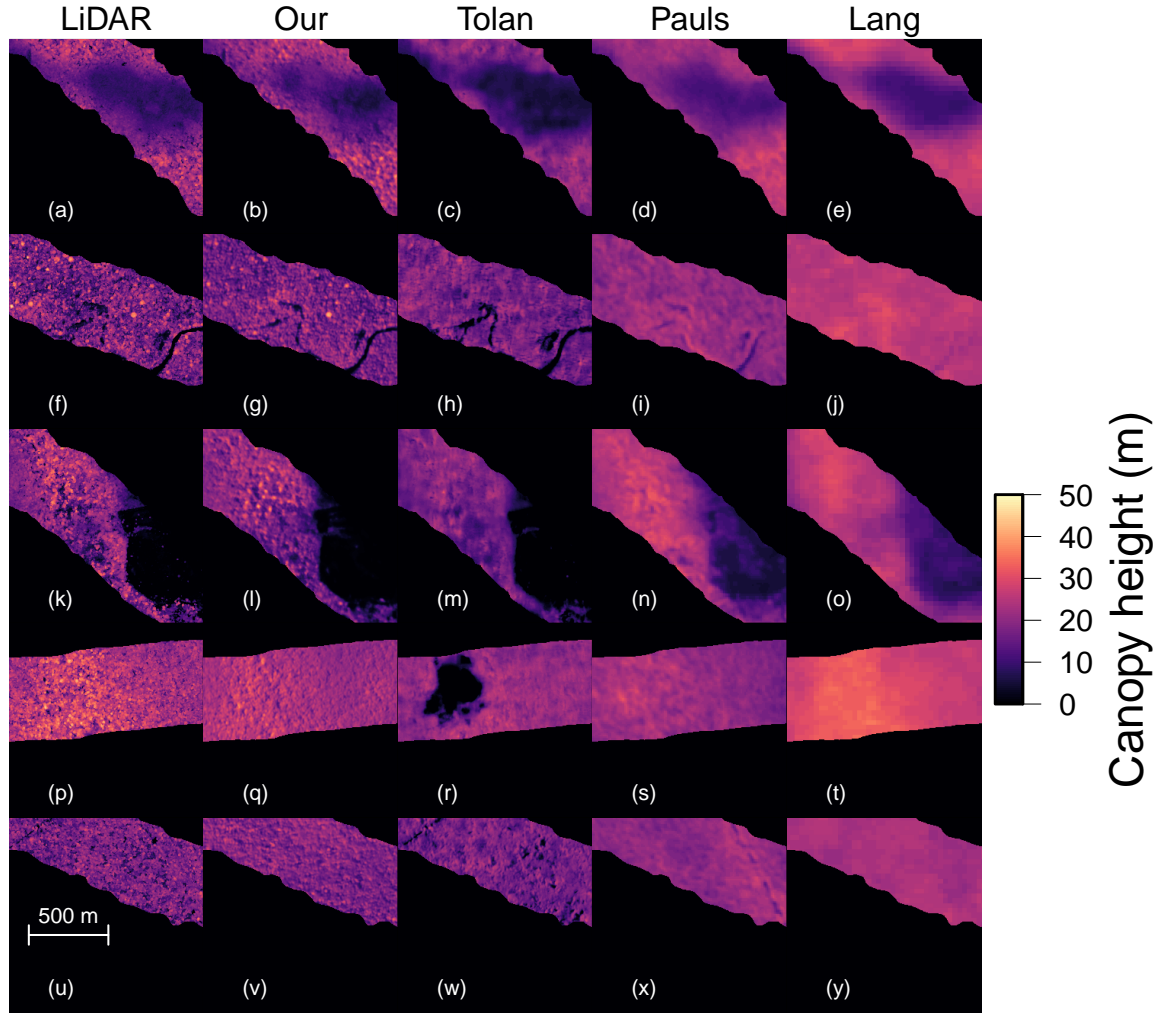


Figure 6. Example of canopy height models observed in the validation dataset (column 1), predicted from our canopy height model (column 2), predicted from Tolan’s model (column 3), and predicted from Lang’s model (column 4). Tolan’s model, Pauls’s model and Lang’s model, whose native spatial resolutions are 0.5 m, 10 m and 10 m, respectively, have been warped to our 4.78 m spatial resolution using the median and nearest neighbor algorithms, respectively.

being misinterpreted by the model as taller vegetation.

The forest can change abruptly in tree height due to clearcuts, Fig. 6k-o. In this scenario, our model captures the forest border well and predicts some isolated trees, Fig. 6l. Tolan’s model also captures the transition, but the CHM appears more blurry and shows fewer isolated trees, Fig. 6m. Pauls’s and Lang’s model show some changes in height but do not reach zero where there is no forest present, Fig. 6n-o.

Smooth changes in height, Fig. 6p-t, are well mapped by our model, Fig. 6q, but with a common cloud artifact in Tolan’s model, Fig. 6r. Pauls’s model looks similar to our results but is a bit more blurry, Fig. 6s. Lang’s model also maps the changes in height well, Fig. 6t.

For forests with small gaps or lines such as roads, Fig. 6u-y, our model struggles to

reach the lower height points, Fig. 6v, while Tolan's model seems to capture them well and even enhances them, Fig. 6w. Pauls's model does not capture the same small gaps and roads, Fig. 6x but capture to a road opened after June 2018 (after our validation sample image was taken). Lang's model does not capture such small-scale gaps, Fig. 6y.

3.4. Height distribution at validation area-level from our model

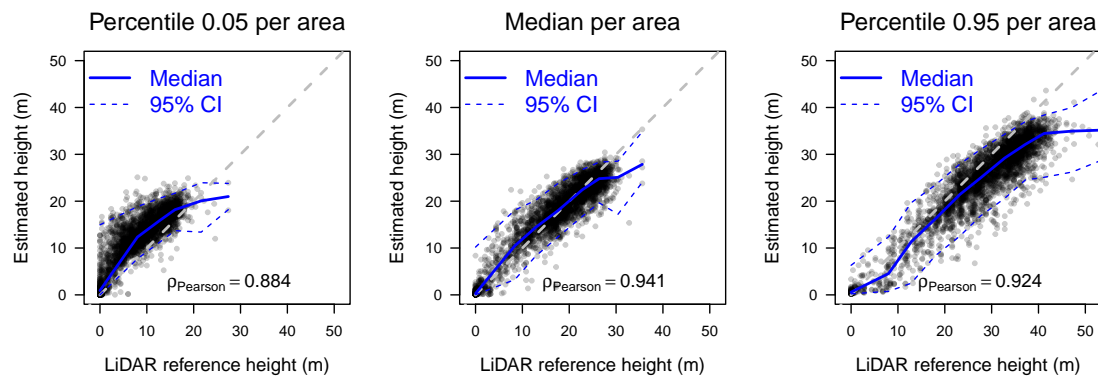


Figure 7. Percentile 0.05 (a), median (b), and percentile 0.95 (c) of heights computed from canopy heights observed and predicted by our model in the 3,436 validation areas. Median of the points and 95% confidence interval computed by intervals of 5 m is given in blue. Each point represents one validation area.

For most validation areas, Fig. 7a, the 5th percentile, while highly correlated with the LiDAR reference, tends to be overestimated when the reference height is above 1-2 m, with more significant errors observed around 5-15 m. Regarding the median (50th percentile, Fig. 7b), the model accurately predicts heights, closely aligning with the 1:1 line, with points well-distributed around it. This is supported by a Pearson correlation coefficient (ρ) of 0.927, higher than that for the other percentiles. For the 95th percentile, Fig. 7c, the model shows a slight underestimation that increases with height, reaching approximately -5 to -10 m for the tallest points. This may be attributed to the fact that the ratio of height to crown size is not consistently preserved with increasing height, meaning taller trees do not necessarily have larger crowns.

3.5. Logging detection from height

The area depicted in Fig. 8, located in Mato Grosso (Brazil), underwent logging activities during the year 2022. Between March (Fig. 8a) and April (Fig. 8b), new logging activities resulted in cleared areas visible in the April RGB images, Fig. 8b. These newly cleared areas appeared below the center and in the top-right quarter of the image. The new logging areas are also visible in the height difference map between March and April (Fig. 8c), despite some noise originating from variations in illumination and geolocation.

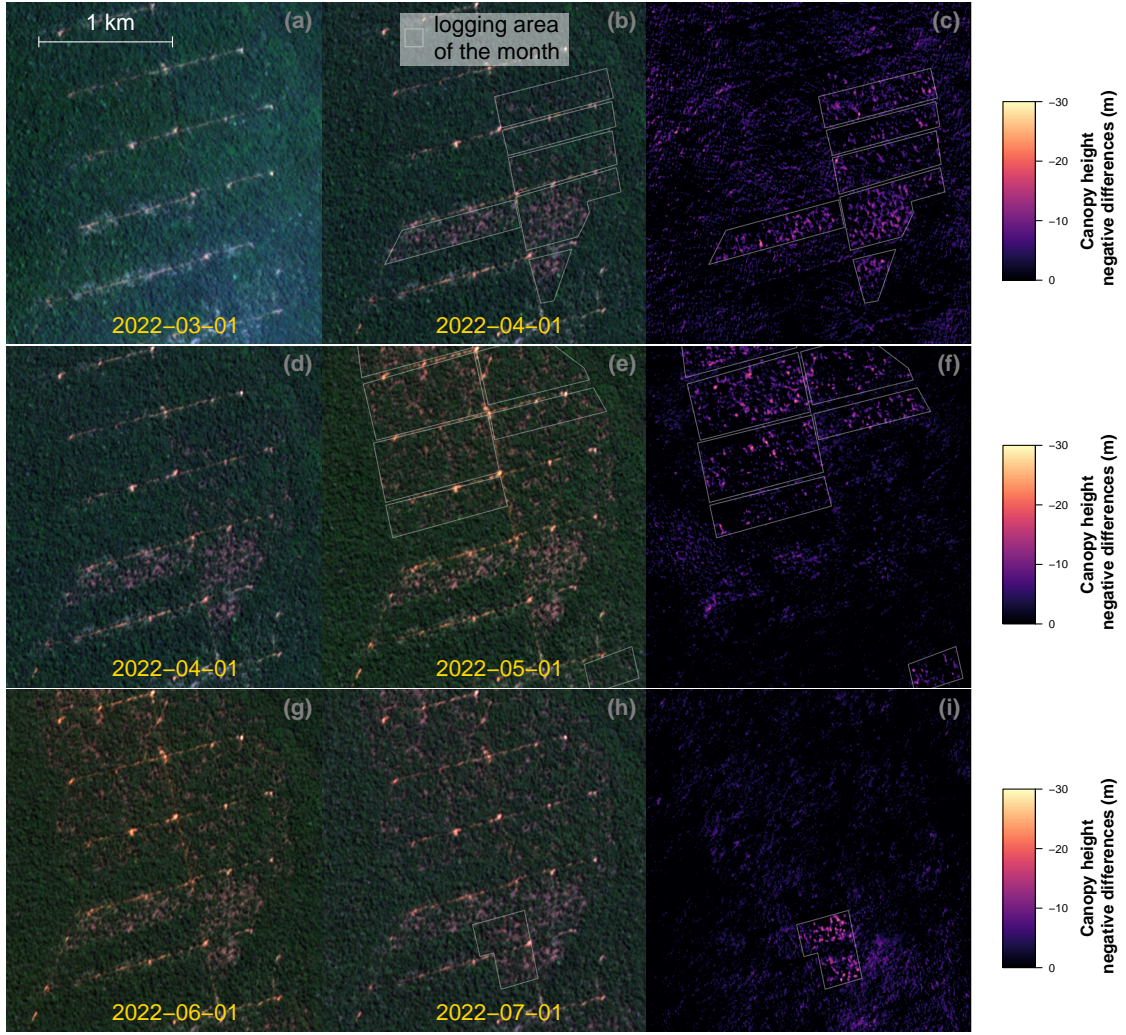


Figure 8. Examples of height changes due to logging activities for the Planet quad 0714-0954 for the periods 2022-03-01 to 2022-04-01 (a-c), 2022-04-01 to 2022-05-01 (d-f), and 2022-06-01 to 2022-07-01 (g-i). Each row of images corresponds to one of these periods and includes: a color composite image of the area (left), a color composite image of the subsequent month showing logging activity (middle), and a canopy height difference map (right). The image size is approximately 2.45 km \times 2.45 km.

For the period April to May, Fig. 8d-e, the logging activity moved to the area above the center of the image. The areas with significant canopy height reduction are clearly marked, indicating the extent of logging activity within this period, Fig. 8f.

For the period June to July, Fig. 8g-h, the logging activity was concentrated in a smaller area below the center of the image. Again, the area with significant canopy height reduction is clearly marked, showing the extent of logging activity within this period, Fig. 8i. Despite noise in the height difference, the month-to-month negative height differences across the area allow us to track the impact of logging over time

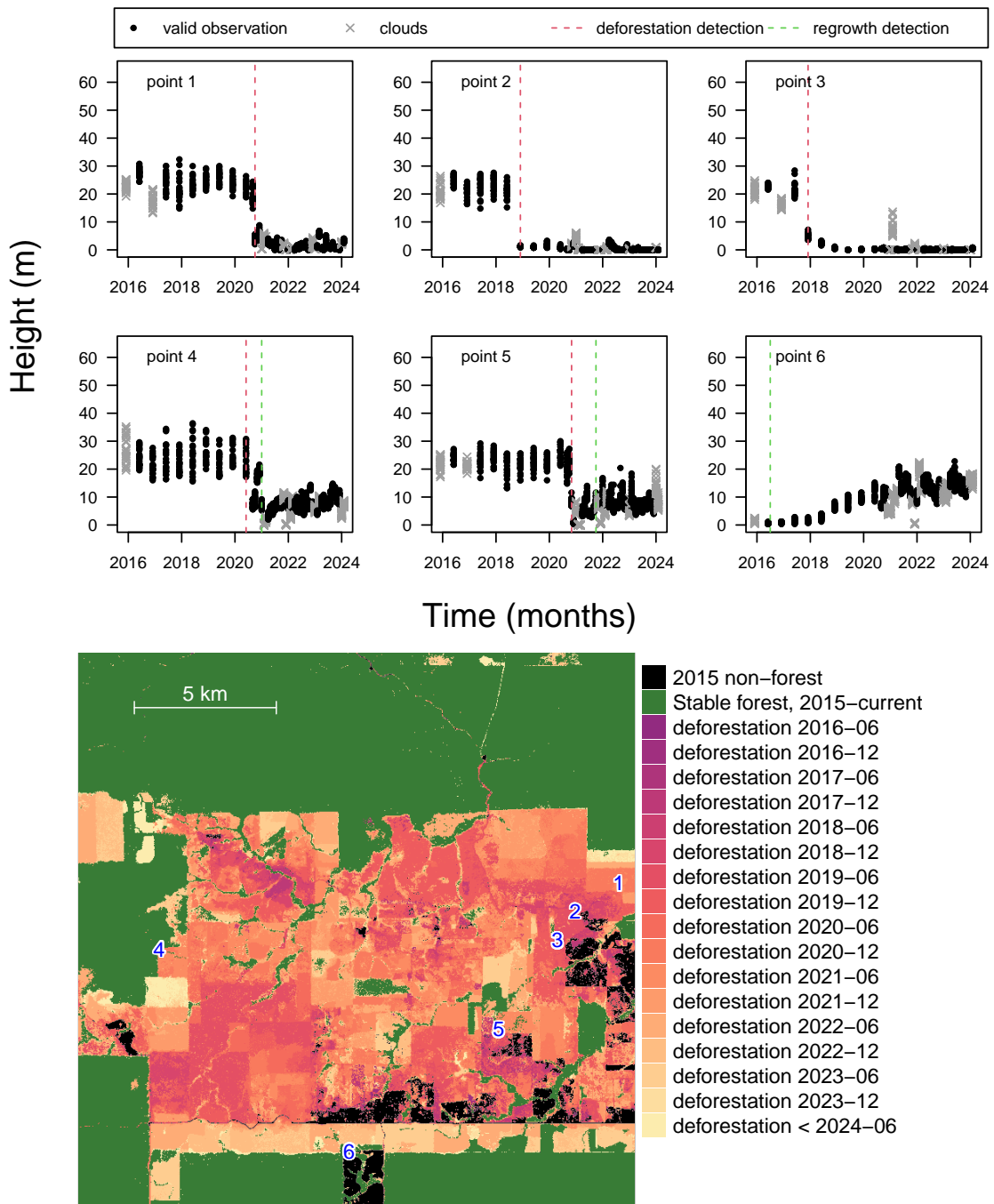


Figure 9. Example of height time series in case of deforestation (points 1, 2, and 3), deforestation and regrowth (points 4, 5) and only regrowth (points 6). For each location, the value of the point and its 24 closest neighbors are presented. The locations of these points are displayed on our previously developed Planet NICFI-based deforestation product for the Planet quad 0681-0967 spanning from December 1, 2015, to February 1, 2024. The Planet NICFI quad covers approximately 19.5×19.5 km.

3.6. Clear-cut and regeneration detection from canopy height

For the selected points in Fig. 9, different patterns of height changes over time are observed for deforestation and regrowth. For point 1, height is relatively stable from 2016 to 2019, followed by a significant drop in height indicating deforestation in 2020. The drop in height occurs at the same time as deforestation is detected by our deforestation algorithm (Wagner et al., 2023; CTrees.org, 2024). After deforestation, the height remains low, and minimal regrowth is observed. For point 2, stable heights are observed until 2017. A sharp decline in height occurs in late 2018, corresponding to the deforestation event, and low regrowth is detected afterward. For point 3, height is stable until mid-2017. A marked decrease around 2018 indicates deforestation, followed by a sustained period of low height values with no significant regrowth. Points 1, 2, and 3 only show deforestation detected by our deforestation/regrowth algorithm (Wagner et al., 2023; CTrees.org, 2024).

For points 4 and 5, regrowth follows a deforestation event, and for point 6, regrowth occurs from cropland (likely an older deforestation). Points 4 and 5 show high heights until around mid-2020. Then, after the deforestation events, some slow regrowth is observed, which is detected by our deforestation/regrowth algorithm. For point 6, low height values are observed at the beginning of the time series. This point was identified as non-forest in 2015. Starting around 2018-2019, low but significant regrowth is observed, and it continues to increase in height through 2024, with some points reaching 15 to 20 m.

The presence of clouds can affect the height by diminishing or increasing it, as observed in all of the time series, Fig. 9.

3.7. Artifacts from clouds and shade

In raw predictions, clouds, haze, shade from clouds, and blur due to image processing create different artifacts, Fig. 10. The model generalizes sufficiently to give good predictions with light haze, such as at location 1 in Fig. 10a-b where individual crowns can be seen. However, for blur in the image, location 2 in Fig. 10a-b, the tree height prediction is underestimated. For clouds and high reflectance values due to clouds, location 3 in Fig. 10a-b, the height diminishes until reaching zero, masking all features of the forest canopy. Finally, for some shaded forests, location 4, heights can appear overestimated. Our cloud mask enables us to discard all errors caused by clouds; for example, the entire image in Fig. 10a is classified as cloudy.

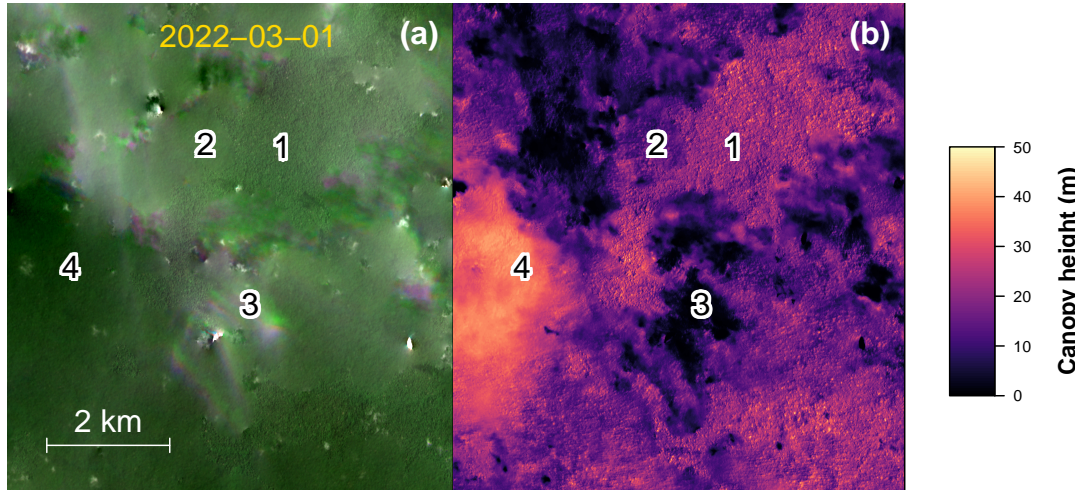


Figure 10. Example of artifacts in height prediction caused by haze, blur, clouds, and shade in the NICFI images before cloud correction for the Planet quad 0722-1038 basemap of 2022-03-01. Location 1 is a hazy but clear part of the image for reference, location 2 is a blurry part of the image, location 3 is a cloudy area with very high reflectance values, and location 4 is a shaded part of the image. Note that this image is classified as 100% clouds after filtering by our cloud model. The image size is $\sim 7.34 \times 7.34$ km.

3.8. Valid observations in Planet NICFI data

Among the 22,063 Planet NICFI tiles covering the Amazon forest, 1,860 (8.06%) contained at least one pixel with no observations. However, all of these 1,860 tiles had at least some pixels with 3 observations. The Planet NICFI time series used here consists of 56 dates. The mean number of cloud-free observations over the Amazon was 32.34, though it varied significantly across space (Fig. 11). The number of observations was higher in the southern part of the Amazon, where it reached a maximum of 55.9 out of a possible 56. The lowest number of mean cloud-free observations was 0.25, located in French Guiana (Planet NICFI quads 0717-1048). More broadly, the lowest mean observation numbers were found in the Guiana Shield, the western part of the Amazon near the Andes, and in the region around the boundary between central and western Amazon. For those regions, we increased the number of observations to compute the mean height by making our cloud/shade masking less restrictive.

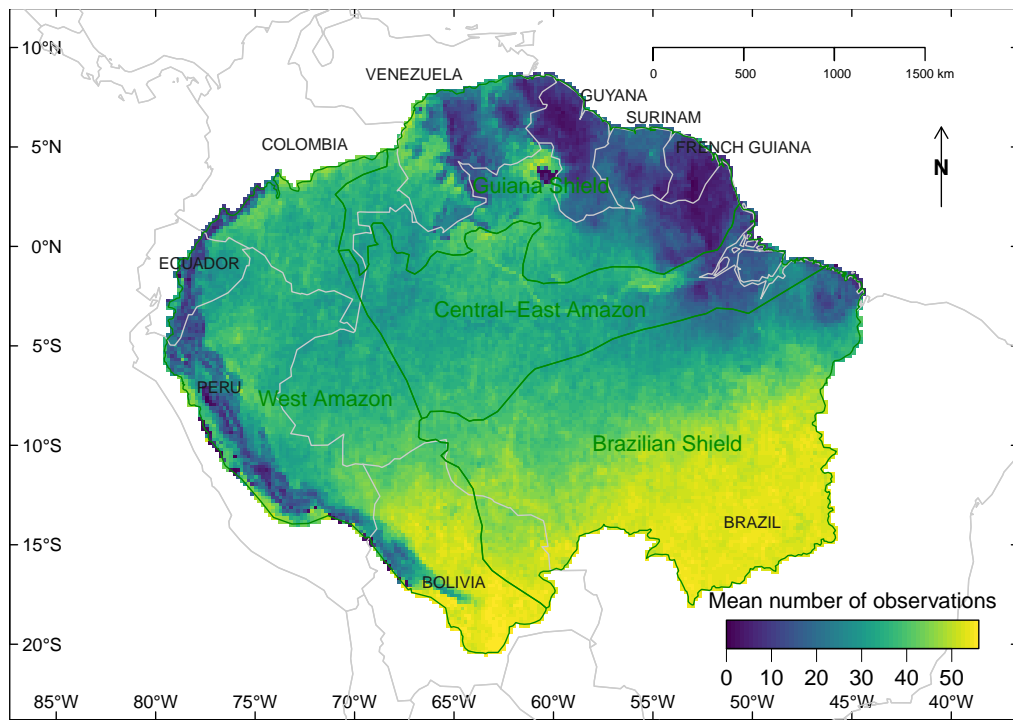


Figure 11. Mean number of cloud-free observations for the $\sim 20 \text{ km} \times 20 \text{ km}$ pixels corresponding to the Planet NICFI tiles. Only pixels with vegetation height greater than zero were considered in the mean computation.

3.9. Amazon forest canopy height

We found that the mean canopy height of the Amazon forest was 22.09 m, with a median of 22.25 m and a 97.5th percentile of 32.10 m (Table 1).

Canopy height Metrics	value (m)
Mean	22.09
Percentile 2.5	11.34
Percentile 5	13.25
Percentile 25	18.75
Median, Percentile 50	22.25
Percentile 75	25.54
Percentile 95	30.54
Percentile 97.5	32.10

Table 1. Amazon forest canopy height descriptive statistics.

The forests with the highest mean height (Fig. 12a) were primarily located in the Eastern part of the Guiana Shield and in the upper part of the West Amazon and along its border with the Central-East Amazon region (Fig. 12a). The the Guiana Shield contains most of the large, continuous regions where mean canopy heights reach up to ~ 30 m.

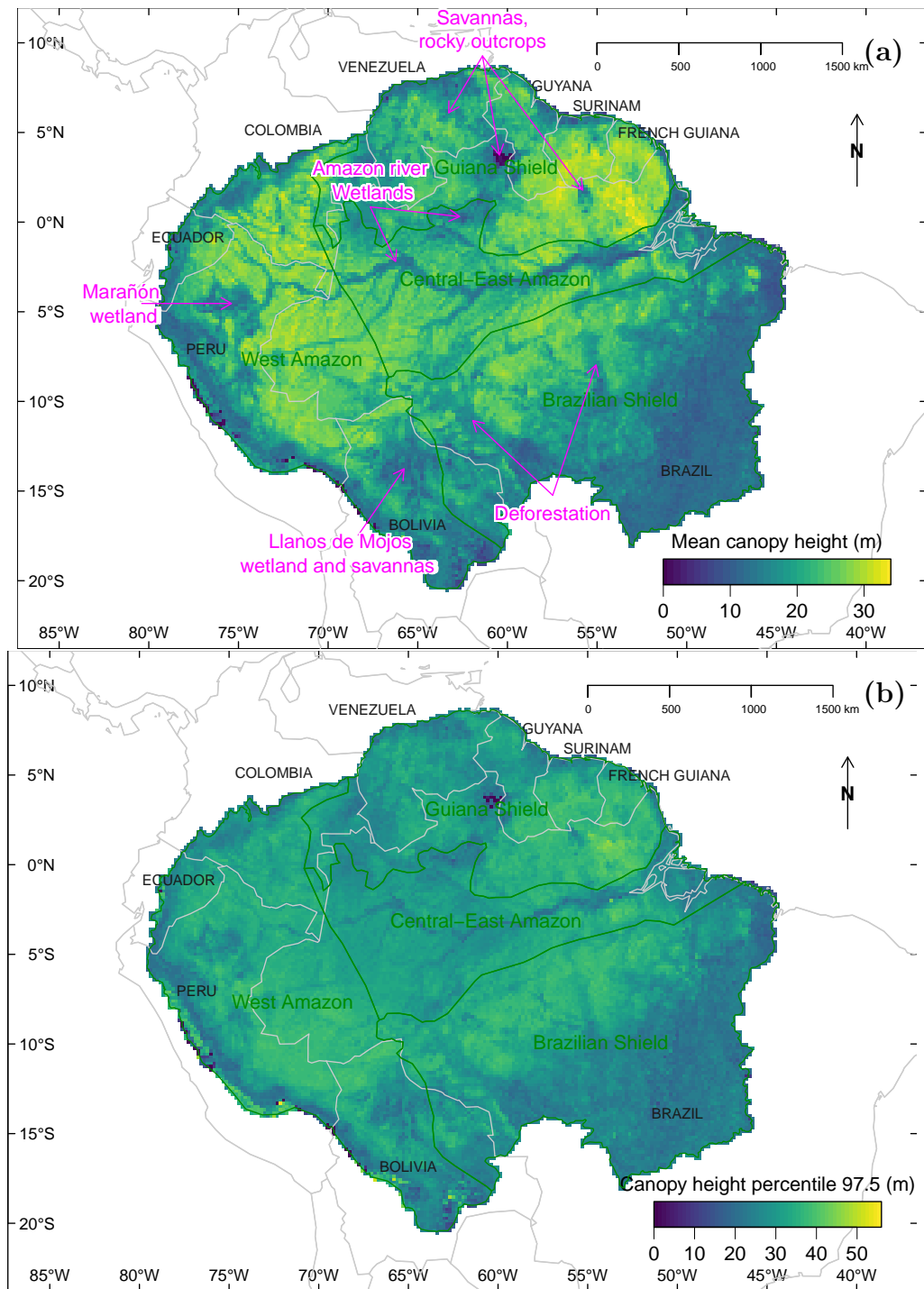


Figure 12. Map of the mean and percentile 97.5th of the Amazon forest tree canopy height on the period 2020-2024 (a-b). Each statistics is given for $\sim 20 \text{ km} \times 20 \text{ km}$ pixels which correspond to a planet tile. Inside a tile, mean and percentile 97.5th are computed only with pixels that have \geq three non-clouded observation.

For the 97.5th percentile (p97.5) of canopy height (Fig. 12b), there is a spatial pattern of the tallest forests. These forests form a circle, up to 1,000 km wide, around the Central Amazon region. Some of these forests have p97.5 values that exceed 50 m, which

is considered exceptionally tall for the Amazon. Within these tall forests, a particular hot spot emerges in the Guyana shield, on the south of the French Guiana and Brazil border. In the east, approximately 500 km before the Amazon reaches the Atlantic, there are large patches of tall forests south of the Amazon River in Brazil. Additionally, significant continuous areas of tall forests are found in the Western Amazon region.

On the western slopes of the Andes, there are no natural forests, only tree plantations; the values (mean and 97.5th) represent only the few plantations within the 20×20 km tiles.

Some patterns of lower canopy height are also observed: (i) shorter forests are found near the Amazon River and wetlands, such as in the Marañón Basin in Peru (the westernmost large tributary of the Amazon River) and the Llanos de Mojos savannas in the Madeira Basin of eastern Bolivia; (ii) near the Andes, where elevation increases and the treeline becomes apparent; (iii) around rock outcrops, such as the Tepuis in Venezuela; (iv) near savannas, where the lowest canopy height regions are located in a savanna ecosystem shared between Brazil, Guyana, and Venezuela; and (v) near deforested areas, including the Arc of Deforestation, with some major low-height regions in the northwest part of the Brazilian shield.

3.10. Comparison with global canopy height products

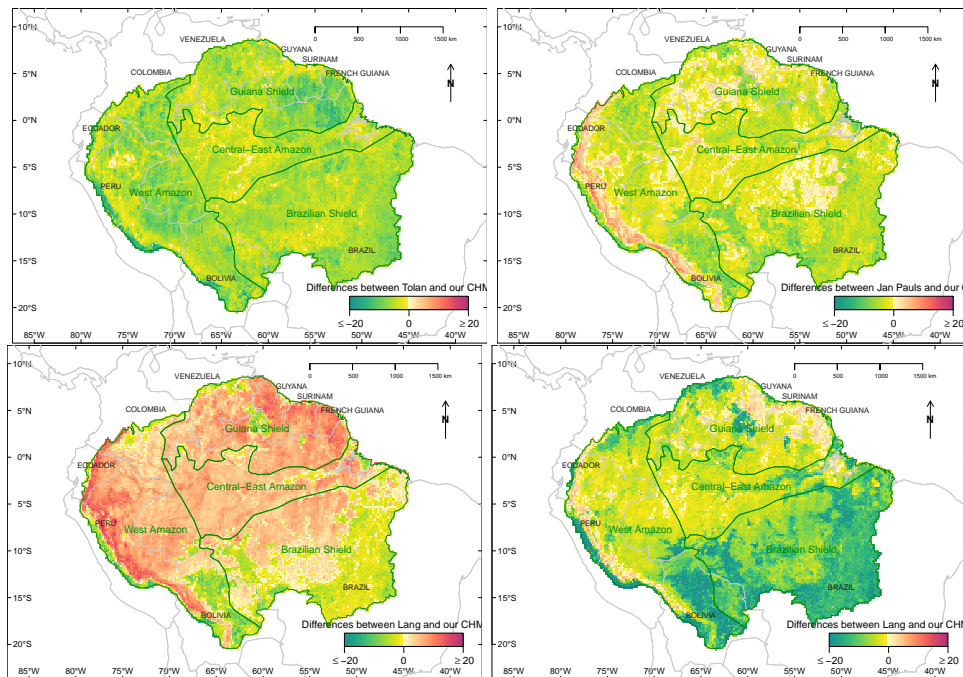


Figure 13. Tree canopy height differences in meters between Tolan's product (a), Pauls's product (b), Lang's product (c-d), and our canopy height product. For Lang's product, we compared it to the mean of our product (c) and the 97.5th percentile (d), as Lang models the GEDI 98% relative height (RH98). Differences are shown for the $\sim 20 \text{ km} \times 20 \text{ km}$ Planet NICFI tiles, considering only pixels with vegetation height greater than zero.

The difference between Tolan's model and our canopy height, Fig. 13a, indicates that our product is close to the Tolan's product, but produces higher canopy heights mostly in the Guyana shield and in the Western Amazon region where trees are taller. This confirms the observation made on the validation sample (Fig. 3b), which shows a saturation of Tolan's CHM slightly above 30 m. The differences show very slight pattern, likely indicating that while Tolan's model does not capture the tallest heights, it still captures very well the variation of height in the landscape.

The difference between Jan Pauls's height and ours is below 10 m for most of the map, Fig. 13b, with some regions showing very similar values. Our product gives same or higher canopy heights for most of the Amazon, except near the Andes, where our model, based on optical data, has fewer valid observations (Fig. 11). Jan Pauls's model is based on both radar and optical data (Sentinel 1 and 2) (Pauls et al., 2024), which may explain why it better captures this region. For fragmented forest region in the arc of deforestation, Jan Pauls's height model systematically underestimates canopy height.

Lang's model, which provides mean RH98 height, shows consistently higher values compared to our mean canopy height data, especially in areas with dense canopy cover, but is lower in areas with less dense forest, Fig. 13c.

The difference between Lang's model mean RH98 height and our 97.5th percentile shows that our 97.5th percentile is mostly higher than Lang's RH98, Fig. 13d. The regions where Lang's model provides higher predictions are located the Guiana Shield and near the Andes. Lang's model is based on Sentinel 2 optical data, which may have more observations over these regions, or the height predictions might benefit from the latitude and longitude variables included in Lang's model. Just like Jan Pauls's height model, Lang's model systematically underestimates canopy height in fragmented or sparse forests such as in the Brazilian arc of deforestation and the southern part of the Amazon.

In conclusion, our model seems to provide better and higher estimates of canopy height across the Amazon, except in regions with very high cloud cover and shade, such as near the Andes.

3.11. Very high resolution map of the Amazon canopy height

The very high-resolution canopy height map of the Amazon forest shows highly diverse and consistent large-scale spatial patterns of tree height (Fig. 14). As observed in the analysis (section 3.9), variables associated with lower heights include (i) natural factors such as wetlands, savannas, and rock outcrops, and (ii) human activities like deforestation and roads. In Brazil, roads are already following the arc of taller forests revealed by the p97.5 canopy height (Fig. 12b), and some large forested areas within this arc have already been deforested and fragmented.

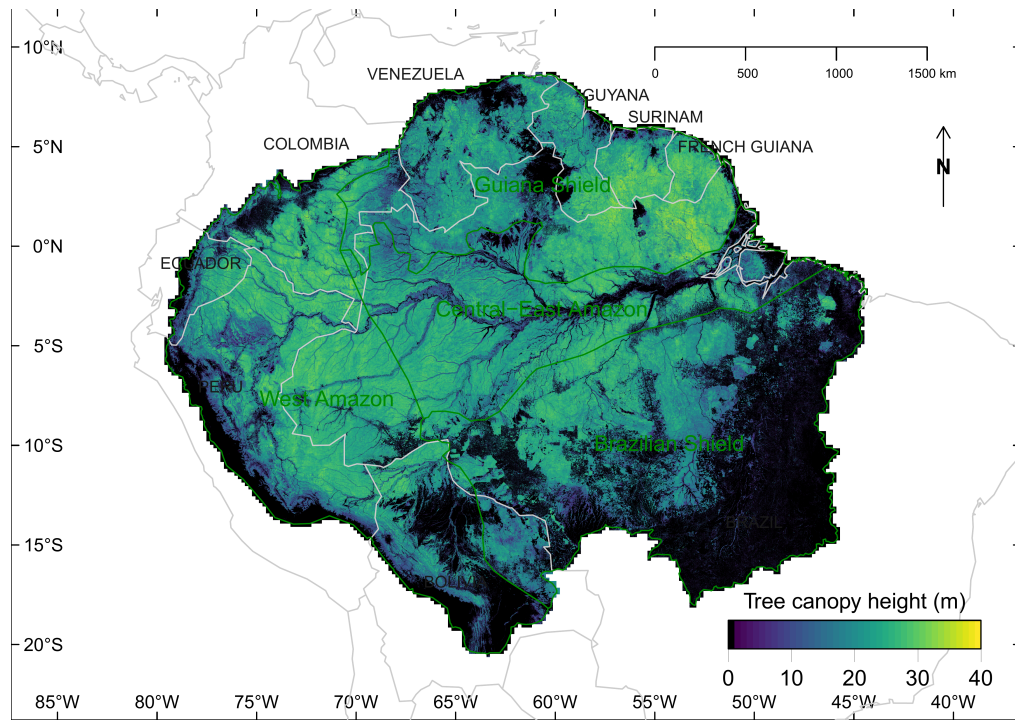


Figure 14. Canopy height of the Amazon forest (m). To facilitate visualization at very high resolution, the colors represent the estimates from our model, aggregated to an 80 m spatial resolution using the median.

For most of the Amazon forest, the model enables the detection of the tallest trees with the largest crowns, Fig. 15. These trees were visually identified by examining groups of pixels above 40 meters across some regions of the Amazon. The first individual, Fig. 15a-c, has a crown diameter of approximately 70 m, making it the largest tree found in our Amazon dataset so far, and likely one of the largest tree crowns in the Amazon forest. All the other trees also have crown diameters above 50 meters, which explains their good visibility in the NICFI image with a spatial resolution of 4.78 m. Each of these trees exhibits distinct annual phenology, with a complete renewal of leaves occurring within 1-2 months every year during the same period (observed from 2021-2024). The species are unknown.

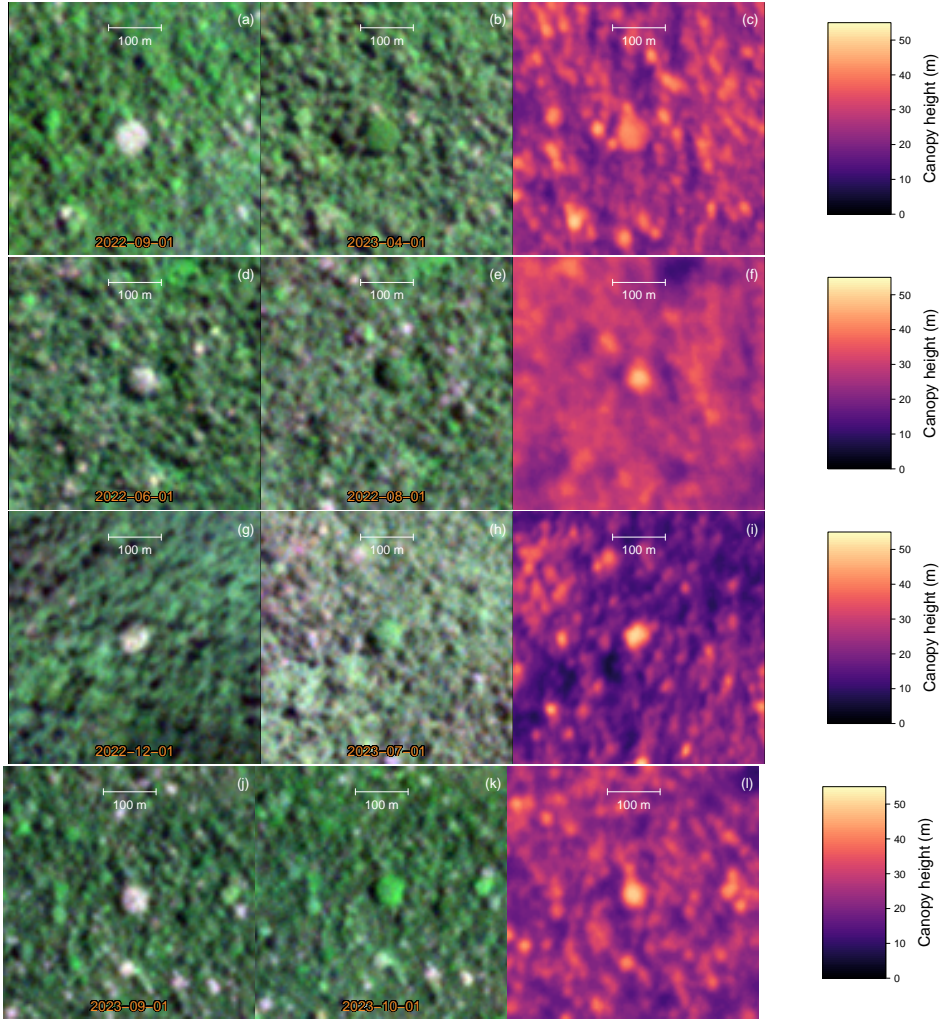


Figure 15. Examples of giant trees identified by our Amazon canopy height model. For each individual tree (row), a Planet NICFI image is shown during its leafless period (first column), during its leaf-covered period (second column), and the third column presents our canopy height composite for the year 2020. The resolution of the NICFI image, preserved in this figure, is 4.78 m.

4. Discussion

In this study, we found that the Amazon forest has a mean canopy height of 22.09 m, a median of 22.25 m, and a 97.5th percentile of 32.10 m. The tallest forests form a 1,000 km-wide arc around the Central Amazon. A canopy height hotspot was identified in the Guiana Shield, near the southern border of French Guiana and Brazil, where the tallest documented Amazon trees, such as a *Dinizia excelsa* reaching 88.5 m, have been recorded (Gorgens et al., 2019). On the Amazon forest scale, the canopy height varies significantly, with shorter forests near rivers, wetlands, savannas, and deforested areas, reflecting local environmental and anthropogenic influences (Fig. 14).

Here, we show that Planet NICFI images with a 4.78 m spatial resolution enable accurate mapping of Amazon forest canopy height, even allowing the identification of

most large tree crowns. The U-Net network, adapted for regression, estimated canopy height with a mean error of 3.68 m on the validation dataset. This confirms the high capacity of convolutional networks to support vegetation mapping, particularly canopy height mapping (Wagner et al., 2024; Kattenborn et al., 2021).

For the Amazon forest, our locally calibrated model provided more accurate canopy height estimates with fewer biases than the currently available global canopy height models (Fig. 3, 4). While this result is expected for lower-resolution global models (Lang et al., 2023; Pauls et al., 2024), it also outperformed Tolan's model at higher resolution, which is made using Maxar Vivid2 mosaic imagery at 0.5 m resolution (Tolan et al., 2024). Our canopy height map, Fig. 14, except for the Andes, shows similar spatial height patterns to those observed in other height maps (Lang et al., 2023; Tolan et al., 2024; Pauls et al., 2024), but reaches greater heights and provides details down to individual crowns.

Some regions exhibit higher canopy heights, such as the Guiana Shield and the western Amazon (Fig. 12b), but the most prominent patterns of canopy height seem to be influenced by edaphic conditions. The lowest heights are observed near wetlands, major rivers, high elevations, rocky outcrops, and savannas, such as those in southern Guyana and the Roraima region (Fig. 12a, Fig. 14). Large-scale height patterns do not appear to directly reflect above-ground biomass variations estimated from field plots, which range from 200–250 Mg.ha⁻¹ in the western Amazon to nearly 400 Mg.ha⁻¹ in some field sites in the central Amazon and Guiana Shield (Malhi et al., 2006; Avitabile et al., 2016). Maximum height seems to represent an upper limit achievable by most Amazon regions under favorable edaphic conditions, regardless of forest basal area or mean wood density, as shown by the 97.5th percentile in Fig. 12a. Finally, our map highlights large-scale human disturbance effects on Amazon forest height, with visible scars of deforestation in the Brazilian Shield and western Amazon region (Fig. 12a, Fig. 14).

The large variability across space of the Amazon forest is observed for species (Luize et al., 2024) as well as forest structure and biomass (de Conto et al., 2024; Saatchi et al., 2011), and the large-scale patterns of height observed in our data reinforce that the Amazon forest is not a uniform and homogeneous forest, for example with the hotspot of high trees in the Guiana Shield, found in this study and in Gorgens et al. (2019). This is particularly concerning for conservation efforts because deforestation that still occurs in the Amazon operates mostly by removing almost entirely large patches of continuous areas of forest, Fig. 14, which is likely the best manner to remove forests that are unique.

We acknowledge that our map could underestimate canopy height in the Andes due to cloud cover and shading issues in the optical data. For this region, estimations from other models, such as Jan Pauls' model using Sentinel-1 radar, which can penetrate through clouds and shade, seem more reliable (Pauls et al., 2024; Lang et al., 2023). We adopted a rigorous cloud-masking strategy to exclude clouds, thin clouds, haze, and image artifacts, adding a buffer of ~1200 m to ensure only very high-quality, cloud-

free pixels were used in the analysis. However, this significantly reduces the number of usable pixels, particularly in regions with frequent or persistent cloud cover. In the next iteration of the model, we will improve it to predict height under thin clouds. This strategy could increase the number of pixels with predictions and enhance the accuracy of the temporal height composite for regions on the Andes slopes.

The Amazon is usually considered a forest with relatively low canopy height among Earth's tropical forests. In our sample, trees can go up to 65–88.5 m for rare taller individuals (Gorgens et al., 2019) (<https://www.smithsonianmag.com/science-nature/researchers-discover-tallest-known-tree-amazon-180973227/>), but the mean canopy height in the sample is ~ 20 m, Fig. 4a, and we found 22.1 m of mean canopy height in the Amazon forest. Globally, if looking at rainforest tree height distribution from GEDI (Bourgoin et al., 2024), canopy heights > 40 m represent 5% in the Amazon rainforest, 10% in African rainforests, and above 25% in Asian rainforests. *Dipterocarp* forests of Southeast Asia are considered the highest tropical forests, with mean heights recorded for a forest of Borneo as high as 50 m, and reaching 98 m for the tallest individual recorded so far (Shenkin et al., 2019) (and see (Shenkin et al., 2019), figure 3A). We acknowledge that our model cannot currently capture these extremely tall trees, but we will further integrate training samples from other tropical forests to build a global canopy tree height model using NICFI data.

The remaining Amazon is still one of the only places to observe natural plants on a large scale in intact landscapes, offering a unique opportunity to document and study one of the last 'pristine' large-scale tropical forests. In this context, our model can already be used to locate the giant trees in the Amazon forest and in forests of similar stature, Fig. 15. Preserving these trees is essential for maintaining biodiversity and the functioning of these forest ecosystems (Piirto and Rogers, 2002; Francis and Asner, 2019; Enquist et al., 2020). The finding of four large trees, Fig. 15, was made by visual inspection of some tiles and the help of a canopy height mask over 40 m. With automatic detection, there is now a potential to map all of the largest trees of the Amazon from our data and analyze their distribution, species, or phenology, as well as plan their protection against near-future risk. Additionally, our map provides an unprecedented description of canopy height heterogeneity in regions where aerial LiDAR is nonexistent, which could help characterize relationships between species occurrence and canopy height and structure (Moudrý et al., 2024).

4.1. Advances in canopy height changes mapping

Currently, changes in tropical forest cover, from deforestation, degradation, or regeneration at regional to global scale with optical data, are mostly made based on the semantic segmentation of the object for each date, for example, forest cover or fire, and the subsequent analysis of the time series of the classified pixels (Hansen et al., 2013; MapBiomass, 2024; Wagner et al., 2023; Dalagnol et al., 2023; Csillik et al., 2019; Heinrich et al., 2021, 2023). In regrowth analysis, the canopy height is not used, and

the algorithm relies on forest cover classification. For example, if a pasture becomes classified as a forest and stays classified as forest for the next 10 years, the pixel is considered a 10-year regenerating secondary forest (Heinrich et al., 2021). This works well for regrowth after large tree cover removal or if the pixel was originally a non-forested pixel, but, if the pixel is logged or degraded, it can lose some height but remain as forested tree cover and unchanged for the algorithm.

The canopy height could help in this case, and the remote sensing community is in the early stages of mapping changes in tropical forest cover using height. For example, in recent work that used height, most of them, such as all open global canopy height products cited in this work, only mapped one date (Lang et al., 2023; Pauls et al., 2024; Tolan et al., 2024; Potapov et al., 2021). Currently, studies using multi-temporal height estimation are mostly using LiDAR data. For example, in the Amazon arc of deforestation, using repeated LiDAR data (some of which are included in our training sample), it was shown that losses in forest height and carbon from anthropogenic and natural processes, as well as growth, could be identified and estimated (Csillik et al., 2024). On a similar dataset, other studies show the dynamics of gaps opening and closing in the Amazon forest, as well as the growth of trees in the gaps (Dalagnol et al., 2021; Winstanley et al., 2024). The only global product doing changes at very high resolution is the Planet Forest Carbon Monitoring (FCM), which provides quarterly updates at 3 m resolution of Canopy Cover, Canopy Height, and Aboveground Live Carbon, but it is commercial and not peer-reviewed.

In this work, we show that the Planet NICFI time series has the potential to be used for mapping changes in canopy cover height at high resolution, Fig. 8 and 9. Our model captures logging activities, Fig. 8, and their impact on forest canopy height. Even though the results can be slightly noisy and some changes are observed outside the logging area (likely natural changes due to phenology), observing this decrease in canopy height is encouraging, as this type of forest disturbance is extremely difficult to estimate from optical remote sensing. Locating where the change appears is feasible currently (Dalagnol et al., 2023), but there is still no means to estimate how much canopy height has changed or how much biomass has been removed. It is also important to have high-frequency time data, such as monthly updates provided by Planet NICFI, to identify the loss, as gaps can close rapidly in tropical forests, sometimes within a few months due to lateral ingrowth, which can mask tree loss (Dalagnol et al., 2021; Winstanley et al., 2024).

Using the time series of height (Fig. 9), deforestation can be observed as a change in height for pixels, providing estimates similar to those for deforestation dates previously identified based on tree cover changes (Wagner et al., 2022). If the forest is converted to pasture, the predicted height remains near zero (Fig. 9 points 1-3), while in cases of regrowth, the height starts to increase (Fig. 9 points 4-5). Growth takes some years to be clearly identified, but a promising result is the detection of secondary forest growth. In our example, (Fig. 9, point 6), the height time series allows us to track the growth of the forest, for a forest regrowing from abandoned pasture in 2016. Though

further analysis and validation are needed, this result is encouraging and could help measure regrowth from open-access NICFI images, something currently only possible with repeated LiDAR and/or commercial data.

4.2. Open data of canopy height

In our dataset, the largest trees are clearly identifiable. This raises questions regarding open data, as sharing such datasets could impact the communities and environments in their surroundings (Bennett et al., 2024). These large trees could be located, for example, on indigenous lands, areas with uncontacted people, public or private lands. Public knowledge of their locations would attract individuals for purposes such as scientific research, tourism, or logging, and it remains difficult to assess the potential benefits and harms of disclosing tree locations.

While many large trees are still in remote places, far from roads or rivers and thus already have a 'protection' by isolation, others near recent deforestation might be only, and ever, known just by the loggers. If such industries desire information about these trees, they often already possess means to acquire it, whether through aerial surveys or field exploration. At the same time, those trees remain unknown to other communities, including people living in those areas, governments, conservationists, and tourism operators, who could promote protection, enhance awareness, or make sustainable use of these unique trees. These trees could be totally protected, or, if used in sustainable eco-tourism, could be part of socio-bioeconomies (SBEs) (Garrett et al., 2024), defined as economies based on the sustainable use and restoration of Amazonian ecosystems, as well as Indigenous and rural livelihood systems in the region.

A potential solution could involve developing a monitoring system to raise awareness about these trees, thereby increasing their protection by making their existence more visible to actors other than the loggers. As more people become aware, these trees, rather than being at greater risk, could actually benefit from the attention and protection brought about by public visibility, in an analogy to the use of public space in cities (Jacobs, 1961).

But as we are unsure of the benefits and more aware of the misuse and harms, our dataset will remain non-open.

5. Conclusion

In this work, we present the canopy height map of the Amazon forest at ~ 4.78 m spatial resolution for the period 2020–2024. We trained a deep learning regression model with the popular CNN architecture U-Net using Planet NICFI RGB-NIR images as input and LiDAR data as a reference for canopy height. We demonstrate that in the Amazon, our model outperforms all existing remote-sensing-derived canopy height maps. The generated canopy height map enables gathering information about the structure of the forest; we found a mean Amazon forest canopy height of 22.1 m, along with individual

information about the largest trees, such as their height and crown size. The tallest tree density was found in the Shield, and tree height was lower near wetlands, major rivers, high elevations, rocky outcrops, and savannas. The next steps are (i) to improve the model to perform better in the cloudiest and most shaded places, (ii) to train it with data from other tropical forests, with an emphasis on locations with known taller forests, and (iii) to apply our method to the entire NICFI image catalog to map tree height and its changes on a pantropical scale.

6. Acknowledgments

The authors wish to thank the Grantham Foundation and High Tide Foundation for their generous gift to UCLA and support to CTrees.org. Part of this work was carried out at the Jet Propulsion Laboratory, California Institute of Technology, under a contract with the National Aeronautics and Space Administration (NASA). Conceptualization, F.H.W., R.D., G.C., S.F. and S.S.; methodology, F.H.W., R.D., G.C., M.C.M.H., S.G. and S.F.; software, F.H.W., S.G., R.D., G.C., S.F. and M.C.M.H.; validation, F.H.W. and L.B.S.T. ; formal analysis, F.H.W. and S.G.; investigation, F.H.W., R.D., G.C., S.G., L.B.S.T., S.F., M.C.M.H. and S.S.; resources, S.S.; data curation, F.H.W., M.C.M.H., S.G., L.B.S.T., M.K. and J.P.H.B.O; writing—original draft preparation, F.H.W.; writing—review and editing, F.H.W., R.D., G.C., M.C.M.H., S.G., L.B.S.T., S.F., M.K., J.P.H.B.O, L.A., C.C., S.P.G-C., S.L., Z.L., A.M., Y.Y., E.G.S., S.R.W., M.B., P.C., S.C.H. and S.S.; visualization, F.H.W. and M.C.M.H.; supervision, S.S.; project administration, S.C.H. and S.S.; funding acquisition, S.C.H. and S.S.

7. Data availability

Planetscope imagery in tropical areas via Norway's International Climate and Forest Initiative (NICFI) satellite data Level 2 programme is available for non-commercial purposes from Planet Labs at <https://www.planet.com/nicfi/>. The LiDAR datasets from the “Sustainable Landscapes - Brazil” publicly available at https://daac.ornl.gov/CMS/guides/LiDAR_Forest_Inventory_Brazil.html and <https://www.paisagenslidar.cnptia.embrapa.br/>. Data and metadata of the EBA (Biomass Estimation of the Amazon) project LiDAR transects across the Brazilian Amazon are publicly available from <https://zenodo.org/records/7636454> and <https://zenodo.org/records/4968706>. The LiDAR dataset covering the São Paulo Metropolitan Region (SPMR) are publicly available and distributed in LAZ files at <https://registry.opendata.aws/pmsp-lidar/>.

References

Abadi, M., Agarwal, A., Barham, P., Brevdo, E., Chen, Z., Citro, C., Corrado, G.S., Davis, A., Dean, J., Devin, M., Ghemawat, S., Goodfellow, I., Harp, A.,

Irving, G., Isard, M., Jia, Y., Jozefowicz, R., Kaiser, L., Kudlur, M., Levenberg, J., Mané, D., Monga, R., Moore, S., Murray, D., Olah, C., Schuster, M., Shlens, J., Steiner, B., Sutskever, I., Talwar, K., Tucker, P., Vanhoucke, V., Vasudevan, V., Viégas, F., Vinyals, O., Warden, P., Wattenberg, M., Wicke, M., Yu, Y., Zheng, X., 2015. TensorFlow: Large-scale machine learning on heterogeneous systems. URL: <https://www.tensorflow.org/>. software available from tensorflow.org.

Allaire, J., Chollet, F., 2016. keras: R Interface to 'Keras'. URL: <https://keras.rstudio.com>. r package version 2.1.4.

Allaire, J., Tang, Y., 2020. tensorflow: R Interface to 'TensorFlow'. URL: <https://CRAN.R-project.org/package=tensorflow>. r package version 2.2.0.

de Almeida, C.A., Maurano, L.E.P., de Morisson Valeriano, D., Camara, G., Vinhas, L., Gomes, A.R., Monteiro, A.M.V., de Almeida Souza, A.A., Rennó, C.D., Silva, D.E., et al., 2021. Methodology for forest monitoring used in prodes and deter projects. CEP 12, 010.

Asner, G.P., Mascaro, J., 2014. Mapping tropical forest carbon: Calibrating plot estimates to a simple lidar metric. *Remote Sensing of Environment* 140, 614–624.

Astola, H., Seitsonen, L., Halme, E., Molinier, M., Lönnqvist, A., 2021. Deep neural networks with transfer learning for forest variable estimation using sentinel-2 imagery in boreal forest. *Remote Sensing* 13, 2392.

Avitabile, V., Herold, M., Heuvelink, G.B., Lewis, S.L., Phillips, O.L., Asner, G.P., Armston, J., Ashton, P.S., Banin, L., Bayol, N., et al., 2016. An integrated pan-tropical biomass map using multiple reference datasets. *Global change biology* 22, 1406–1420.

Bastin, J.F., Finegold, Y., Garcia, C., Mollicone, D., Rezende, M., Routh, D., Zohner, C.M., Crowther, T.W., 2019. The global tree restoration potential. *Science* 365, 76–79.

Bennett, M.M., Gleason, C.J., Tellman, B., Alvarez Leon, L.F., Friedrich, H.K., Ovienmhada, U., Mathews, A.J., 2024. Bringing satellites down to Earth: Six steps to more ethical remote sensing. *Global Environmental Change Advances* 2, 100003. URL: <https://www.sciencedirect.com/science/article/pii/S2950138523000037>, doi:<https://doi.org/10.1016/j.gecadv.2023.100003>.

Bourgoin, C., Ceccherini, G., Girardello, M., Vancutsem, C., Avitabile, V., Beck, P., Beuchle, R., Blanc, L., Duveiller, G., Migliavacca, M., et al., 2024. Human degradation of tropical moist forests is greater than previously estimated. *Nature* , 1–7.

Chollet, F., Allaire, J., 2018. Deep Learning with R. Manning Publications Co.

Chollet, F., et al., 2015. Keras. <https://keras.io>.

de Conto, T., Armston, J., Dubayah, R., 2024. Characterizing the structural complexity of the earth's forests with spaceborne lidar. *Nature Communications* 15, 8116. URL:

<https://doi.org/10.1038/s41467-024-52468-2>, doi:10.1038/s41467-024-52468-2.

Csillik, O., Keller, M., Longo, M., Ferraz, A., Rangel Pinagé, E., Görgens, E.B., Ometto, J.P., Silgueiro, V., Brown, D., Duffy, P., et al., 2024. A large net carbon loss attributed to anthropogenic and natural disturbances in the amazon arc of deforestation. *Proceedings of the National Academy of Sciences* 121, e2310157121.

Csillik, O., Kumar, P., Mascaro, J., O'Shea, T., Asner, G.P., 2019. Monitoring tropical forest carbon stocks and emissions using planet satellite data. *Scientific reports* 9, 1–12.

CTrees.org, 2024. Redd+ai: Tree cover loss and degradation from logging, fire and roads in tropical forests - v 1.0. URL: <https://xxx/xxx/xxx>. (accessed on dd/mm/yyyy).

Dalagnol, R., Wagner, F.H., Galvão, L.S., Braga, D., Osborn, F., da Conceição Bispo, P., Payne, M., Junior, C.S., Favrichon, S., Silgueiro, V., et al., 2023. Mapping tropical forest degradation with deep learning and planet nicfi data. *Remote Sensing of Environment* 298, 113798.

Dalagnol, R., Wagner, F.H., Galvão, L.S., Streher, A.S., Phillips, O.L., Gloor, E., Pugh, T.A., Ometto, J.P., Aragão, L.E., 2021. Large-scale variations in the dynamics of amazon forest canopy gaps from airborne lidar data and opportunities for tree mortality estimates. *Scientific reports* 11, 1–14.

Dos-Santos, M., Keller, M., Pinage, E., Morton, D., 2022. Forest inventory and biophysical measurements, brazilian amazon, 2009-2018. ORNL DAAC .

Dubayah, R., Blair, J.B., Goetz, S., Fatooyinbo, L., Hansen, M., Healey, S., Hofton, M., Hurt, G., Kellner, J., Luthcke, S., et al., 2020. The global ecosystem dynamics investigation: High-resolution laser ranging of the earth's forests and topography. *Science of remote sensing* 1, 100002.

Enquist, B.J., Abraham, A.J., Harfoot, M.B., Malhi, Y., Doughty, C.E., 2020. The megabiota are disproportionately important for biosphere functioning. *Nature Communications* 11, 699.

Fayad, I., Ciais, P., Schwartz, M., Wigneron, J.P., Baghdadi, N., de Truchis, A., d'Aspremont, A., Frappart, F., Saatchi, S., Pellissier-Tanon, A., Bazzi, H., 2023. Vision transformers, a new approach for high-resolution and large-scale mapping of canopy heights. [arXiv:2304.11487](https://arxiv.org/abs/2304.11487).

Feldpausch, T.R., Banin, L., Phillips, O.L., Baker, T.R., Lewis, S.L., Quesada, C.A., Affum-Baffoe, K., Arends, E.J., Berry, N.J., Bird, M., et al., 2011. Height-diameter allometry of tropical forest trees. *Biogeosciences* 8, 1081–1106.

Francis, E.J., Asner, G.P., 2019. High-resolution mapping of redwood (*sequoia sempervirens*) distributions in three californian forests. *Remote Sensing* 11. URL: <https://www.mdpi.com/2072-4292/11/3/351>, doi:10.3390/rs11030351.

Garrett, R., Ferreira, J., Abramovay, R., Brandão, J., Brondizio, E., Euler, A., Pinedo, D., Porro, R., Cabrera Rocha, E., Sampaio, O., Schmink, M., Torres, B., Varese,

M., 2024. Transformative changes are needed to support socio-bioeconomies for people and ecosystems in the amazon. *Nature Ecology & Evolution* URL: <https://doi.org/10.1038/s41559-024-02467-9>, doi:10.1038/s41559-024-02467-9.

GDAL/OGR contributors, 2019. GDAL/OGR Geospatial Data Abstraction software Library. Open Source Geospatial Foundation. URL: <https://gdal.org>.

Ge, S., Gu, H., Su, W., Praks, J., Antropov, O., 2022. Improved semisupervised unet deep learning model for forest height mapping with satellite sar and optical data. *IEEE Journal of Selected Topics in Applied Earth Observations and Remote Sensing* 15, 5776–5787.

Gloor, M., Brienen, R.J., Galbraith, D., Feldpausch, T.R., Schöngart, J., Guyot, J.L., Espinoza, J.C., Lloyd, J., Phillips, O.L., 2013. Intensification of the amazon hydrological cycle over the last two decades. *Geophysical Research Letters* 40, 1729–1733.

Gorgens, E.B., Motta, A.Z., Assis, M., Nunes, M.H., Jackson, T., Coomes, D., Rosette, J., Oliveira, L.E., Aragão, C., Ometto, J.P., 2019. The giant trees of the amazon basin. *Frontiers in Ecology and the Environment* 17, 373–374.

Hansen, M.C., Potapov, P.V., Moore, R., Hancher, M., Turubanova, S.A., Tyukavina, A., Thau, D., Stehman, S.V., Goetz, S.J., Loveland, T.R., Kommareddy, A., Egorov, A., Chini, L., Justice, C.O., Townshend, J.R.G., 2013. High-resolution global maps of 21st-century forest cover change. *Science* 342, 850–853. URL: <http://science.sciencemag.org/content/342/6160/850>, doi:10.1126/science.1244693, arXiv:<http://science.sciencemag.org/content/342/6160/850.full.pdf>.

Heinrich, V.H., Dalagnol, R., Cassol, H.L., Rosan, T.M., de Almeida, C.T., Silva Junior, C.H., Campanharo, W.A., House, J.I., Sitch, S., Hales, T.C., et al., 2021. Large carbon sink potential of secondary forests in the brazilian amazon to mitigate climate change. *Nature communications* 12, 1–11.

Heinrich, V.H., Vancutsem, C., Dalagnol, R., Rosan, T.M., Fawcett, D., Silva-Junior, C.H., Cassol, H.L., Achard, F., Jucker, T., Silva, C.A., et al., 2023. The carbon sink of secondary and degraded humid tropical forests. *Nature* 615, 436–442.

Huang, D., Tang, Y., Qin, R., 2022. An evaluation of planetscope images for 3d reconstruction and change detection—experimental validations with case studies. *GIScience & Remote Sensing* 59, 744–761.

Hubbell, S.P., He, F., Condit, R., Borda-de Água, L., Kellner, J., Ter Steege, H., 2008. How many tree species are there in the amazon and how many of them will go extinct? *Proceedings of the National Academy of Sciences* 105, 11498–11504.

Illarionova, S., Shadrin, D., Ignatiev, V., Shayakhmetov, S., Trekin, A., Oseledets, I., 2022. Estimation of the canopy height model from multispectral satellite imagery with convolutional neural networks. *IEEE Access* 10, 34116–34132.

Jacobs, J., 1961. *The Death and Life of Great American Cities*. Random House Inc, New York.

Karatsiolis, S., Kamilaris, A., Cole, I., 2021. Img2ndsm: Height estimation from single airborne rgb images with deep learning. *Remote Sensing* 13, 2417.

Kattenborn, T., Leitloff, J., Schiefer, F., Hinz, S., 2021. Review on convolutional neural networks (cnn) in vegetation remote sensing. *ISPRS Journal of Photogrammetry and Remote Sensing* 173, 24–49. URL: <https://www.sciencedirect.com/science/article/pii/S0924271620303488>, doi:<https://doi.org/10.1016/j.isprsjprs.2020.12.010>.

Lang, N., Jetz, W., Schindler, K., Wegner, J.D., 2023. A high-resolution canopy height model of the earth. *Nature Ecology & Evolution* 7, 1778–1789.

Lang, N., Schindler, K., Wegner, J.D., 2019. Country-wide high-resolution vegetation height mapping with sentinel-2. *Remote Sensing of Environment* 233, 111347.

Lapola, D., Pinho, P., Barlow, J., Aragão, L., Berenguer, E., Carmenta, R., Liddy, H., Seixas, H., Silva, C., Silva-Junior, C., et al., 2023. The drivers and impacts of amazon forest degradation, *science*, 379, eabp8622.

LeCun, Y., Bengio, Y., Hinton, G., 2015. Deep learning. *nature* 521, 436–444.

Li, S., Brandt, M., Fensholt, R., Kariyaa, A., Igel, C., Gieseke, F., Nord-Larsen, T., Oehmcke, S., Carlsen, A.H., Junttila, S., Tong, X., d'Aspremont, A., Ciais, P., 2023. Deep learning enables image-based tree counting, crown segmentation, and height prediction at national scale. *PNAS Nexus* 2. doi:[10.1093/pnasnexus/pgad076](https://doi.org/10.1093/pnasnexus/pgad076).

Li, X., Wang, M., Fang, Y., 2020. Height estimation from single aerial images using a deep ordinal regression network. *IEEE Geoscience and Remote Sensing Letters* 19, 1–5.

Lim, K., Treitz, P., Wulder, M., St-Onge, B., Flood, M., 2003. Lidar remote sensing of forest structure. *Progress in physical geography* 27, 88–106.

Liu, S., Brandt, M., Nord-Larsen, T., Chave, J., Reiner, F., Lang, N., Tong, X., Ciais, P., Igel, C., Li1, S., Mugabowindekwe, M., Saatchi, S., Yue, Y., Chen, Z., Fensholt, R., 2023. The overlooked contribution of trees outside forests to tree cover and woody biomass across europe. PREPRINT (Version 1) available at Research Square [<https://doi.org/10.21203/rs.3.rs-2573442/v1>] .

Longo, M., Keller, M., dos Santos, M.N., Leitold, V., Pinagé, E.R., Baccini, A., Saatchi, S., Nogueira, E.M., Batistella, M., Morton, D.C., 2016. Aboveground biomass variability across intact and degraded forests in the brazilian amazon. *Global Biogeochemical Cycles* 30, 1639–1660.

Luize, B.G., Tuomisto, H., Ekelschot, R., Dexter, K.G., Amaral, I.L.d., Coelho, L.d.S., Matos, F.D.d.A., Lima Filho, D.d.A., Salomão, R.P., Wittmann, F., et al., 2024. The biogeography of the amazonian tree flora. *Communications biology* 7, 1240.

LV, G., J, M., LS, B., N, R.C., AP, A., et al, 2021. Science panel for the amazon. CROSS-CHAPTER–THE AMAZON CARBON BUDGET 4 .

Malhi, Y., Wood, D., Baker, T.R., Wright, J., Phillips, O.L., Cochrane, T., Meir, P., Chave, J., Almeida, S., Arroyo, L., et al., 2006. The regional variation of aboveground live biomass in old-growth amazonian forests. *Global Change Biology* 12, 1107–1138.

MapBiomass, 2024. Project MapBiomass, Collection 8.0 of Brazilian Land Cover & Use Map Series. Technical Report. MapBiomass. URL: <https://brasil.mapbiomas.org/colecoes-mapbiomas/>.

Marengo, J.A., Espinoza, J.C., 2016. Extreme seasonal droughts and floods in amazonia: causes, trends and impacts. *International Journal of Climatology* 36, 1033–1050.

Matricardi, E.A.T., Skole, D.L., Costa, O.B., Pedlowski, M.A., Samek, J.H., Miguel, E.P., 2020. Long-term forest degradation surpasses deforestation in the brazilian amazon. *Science* 369, 1378–1382.

Meta and World Resources Institute (WRI), 2023. High Resolution Canopy Height Maps by WRI and Meta was accessed on 18-04-2023 from <https://registry.opendata.aws/dataforgood-fb-forests>. Meta and World Resources Institute (WRI) - 2023. High Resolution Canopy Height Maps (CHM). Source imagery for CHM © 2016 Maxar. Accessed 18-04-2023.

Mo, L., Zohner, C.M., Reich, P.B., Liang, J., De Miguel, S., Nabuurs, G.J., Renner, S.S., van den Hoogen, J., Araza, A., Herold, M., et al., 2023. Integrated global assessment of the natural forest carbon potential. *Nature* 624, 92–101.

Moudrý, V., Gábor, L., Marselis, S., Pracná, P., Barták, V., Prošek, J., Navrátilová, B., Novotný, J., Potůčková, M., Gdulová, K., Crespo-Peremarch, P., Komárek, J., Malavasi, M., Rocchini, D., Ruiz, L.A., Torralba, J., Torresani, M., Cazzolla Gatti, R., Wild, J., 2024. Comparison of three global canopy height maps and their applicability to biodiversity modeling: Accuracy issues revealed. *Eco-sphere* 15, e70026. URL: <https://esajournals.onlinelibrary.wiley.com/doi/abs/10.1002/ecs2.70026>, doi:<https://doi.org/10.1002/ecs2.70026>, arXiv:<https://esajournals.onlinelibrary.wiley.com/doi/pdf/10.1002/ecs2.70026>.

Mouselimis, L., 2022. PlanetNICFI: Processing of the 'Planet NICFI' Satellite Imagery using R. URL: <https://CRAN.R-project.org/package=PlanetNICFI>. r package version 1.0.4 using Imagery 2021 Planet Labs Inc. All use subject to the Participant License Agreement.

National Institute for Space Research (INPE), Earth Observation General Coordination, 2024. MONITORING PROGRAM OF THE AMAZON AND OTHER BIOMES. Deforestation – Legal Amazon. Technical Report. INPE. URL: Available at <https://terrabrasilis.dpi.inpe.br/downloads/> (accessed on 06 August 2024).

Ometto, J.P., Gorgens, E.B., de Souza Pereira, F.R., Sato, L., de Assis, M.L.R., Cantinho, R., Longo, M., Jacon, A.D., Keller, M., 2023. A biomass map of the brazilian amazon from multisource remote sensing. *Scientific Data* 10, 668.

Pan, Y., Birdsey, R.A., Phillips, O.L., Houghton, R.A., Fang, J., Kauppi, P.E., Keith, H., Kurz, W.A., Ito, A., Lewis, S.L., et al., 2024. The enduring world forest carbon sink. *Nature* 631, 563–569.

Pauls, J., Zimmer, M., Kelly, U.M., Schwartz, M., Saatchi, S., Ciais, P., Pokutta, S., Brandt, M., Gieseke, F., 2024. Estimating canopy height at scale. [arXiv:2406.01076](https://arxiv.org/abs/2406.01076).

Piirto, D.D., Rogers, R.R., 2002. An ecological basis for managing giant sequoia ecosystems. *Environmental Management* 30, 110–128.

Planet, 2021. Planet imagery product specifications. Planet Labs: San Francisco, CA, USA , 91.

Planet Team, 2017. Planet application program interface: In space for life on earth. URL: <https://api.planet.com>.

Pooja Pandey, Joe Kington, A.K., Curdoglo., M., 2021. Addendum to planet basemaps. product specifications. nicfi basemaps. v02. NICFI Basemaps .

Potapov, P., Li, X., Hernandez-Serna, A., Tyukavina, A., Hansen, M.C., Kommareddy, A., Pickens, A., Turubanova, S., Tang, H., Silva, C.E., et al., 2021. Mapping global forest canopy height through integration of gedi and landsat data. *Remote Sensing of Environment* 253, 112165.

R Core Team, 2016. R: A Language and Environment for Statistical Computing. R Foundation for Statistical Computing. Vienna, Austria. URL: <https://www.R-project.org/>.

Ronneberger, O., Fischer, P., Brox, T., 2015. U-net: Convolutional networks for biomedical image segmentation. CoRR abs/1505.04597. URL: <http://arxiv.org/abs/1505.04597>, [arXiv:1505.04597](https://arxiv.org/abs/1505.04597).

Rosan, T.M., Sitch, S., O'sullivan, M., Basso, L.S., Wilson, C., Silva, C., Gloor, E., Fawcett, D., Heinrich, V., Souza, J.G., et al., 2024. Synthesis of the land carbon fluxes of the amazon region between 2010 and 2020. *Communications Earth & Environment* 5, 46.

Roussel, J.R., Auty, D., 2021. Airborne LiDAR Data Manipulation and Visualization for Forestry Applications. URL: <https://cran.r-project.org/package=lidR>. r package version 3.2.2.

Roussel, J.R., Auty, D., Coops, N.C., Tompalski, P., Goodbody, T.R., Meador, A.S., Bourdon, J.F., de Boissieu, F., Achim, A., 2020. lidr: An r package for analysis of airborne laser scanning (als) data. *Remote Sensing of Environment* 251, 112061. URL: <https://www.sciencedirect.com/science/article/pii/S0034425720304314>, doi:10.1016/j.rse.2020.112061.

Saatchi, S.S., Harris, N.L., Brown, S., Lefsky, M., Mitchard, E.T., Salas, W., Zutta, B.R., Buermann, W., Lewis, S.L., Hagen, S., et al., 2011. Benchmark map of forest carbon stocks in tropical regions across three continents. *Proceedings of the national academy of sciences* 108, 9899–9904.

Schwartz, M., Ciais, P., De Truchis, A., Chave, J., Ottlé, C., Vega, C., Wigneron, J.P., Nicolas, M., Jouaber, S., Liu, S., Brandt, M., Fayad, I., 2023. Forms: Forest multiple source height, wood volume, and biomass maps in france at 10 to 30 m resolution based on sentinel-1, sentinel-2, and global ecosystem dynamics investigation

(gedi) data with a deep learning approach. *Earth System Science Data* 15, 4927–4945. URL: <https://essd.copernicus.org/articles/15/4927/2023/>, doi:10.5194/essd-15-4927-2023.

Schwartz, M., Ciais, P., Ottlé, C., De Truchis, A., Vega, C., Fayad, I., Brandt, M., Fensholt, R., Baghdadi, N., Morneau, F., Morin, D., Guyon, D., Dayau, S., Wigneron, J.P., 2024. High-resolution canopy height map in the landes forest (france) based on gedi, sentinel-1, and sentinel-2 data with a deep learning approach. *International Journal of Applied Earth Observation and Geoinformation* 128, 103711. URL: <https://www.sciencedirect.com/science/article/pii/S1569843224000657>, doi:<https://doi.org/10.1016/j.jag.2024.103711>.

Shenkin, A., Chandler, C.J., Boyd, D.S., Jackson, T., Disney, M., Majalap, N., Nilus, R., Foody, G., bin Jami, J., Reynolds, G., Wilkes, P., Cutler, M.E.J., van der Heijden, G.M.F., Burslem, D.F.R.P., Coomes, D.A., Bentley, L.P., Malhi, Y., 2019. The world's tallest tropical tree in three dimensions. *Frontiers in Forests and Global Change* 2. URL: <https://www.frontiersin.org/journals/forests-and-global-change/articles/10.3389/ffgc.2019.00032>, doi:10.3389/ffgc.2019.00032.

da Silva, S.S., Brown, F., de Oliveira Sampaio, A., Silva, A.L.C., dos Santos, N.C.R.S., Lima, A.C., de Souza Aquino, A.M., da Costa Silva, P.H., do Vale Moreira, J.G., Oliveira, I., et al., 2023. Amazon climate extremes: Increasing droughts and floods in brazil's state of acre. *Perspectives in Ecology and Conservation* 21, 311–317.

Silva Junior, C.H., Heinrich, V.H., Freire, A.T., Broggio, I.S., Rosan, T.M., Doblas, J., Anderson, L.O., Rousseau, G.X., Shimabukuro, Y.E., Silva, C.A., et al., 2020. Benchmark maps of 33 years of secondary forest age for brazil. *Scientific data* 7, 269.

Skidmore, A.K., Coops, N.C., Neinavaz, E., Ali, A., Schaepman, M.E., Paganini, M., Kissling, W.D., Vihervaara, P., Darvishzadeh, R., Feilhauer, H., et al., 2021. Priority list of biodiversity metrics to observe from space. *Nature ecology & evolution* 5, 896–906.

Ter Steege, H., Pitman, N.C., Sabatier, D., Baraloto, C., Salomão, R.P., Guevara, J.E., Phillips, O.L., Castilho, C.V., Magnusson, W.E., Molino, J.F., et al., 2013. Hyperdominance in the amazonian tree flora. *Science* 342, 1243092.

Tolan, J., Yang, H.I., Nosarzewski, B., Couairon, G., Vo, H.V., Brandt, J., Spore, J., Majumdar, S., Haziza, D., Vamaraju, J., Moutakanni, T., Bojanowski, P., Johns, T., White, B., Tiecke, T., Couprie, C., 2024. Very high resolution canopy height maps from RGB imagery using self-supervised vision transformer and convolutional decoder trained on aerial lidar. *Remote Sensing of Environment* 300, 113888.

Wagner, F.H., Dalagnol, R., Silva-Junior, C.H.L., Carter, G., Ritz, A.L., Hirye, M.C.M., Ometto, J.P.H.B., Saatchi, S., 2023. Mapping tropical forest cover and deforestation with planet nicipi satellite images and deep learning in mato grosso state (brazil) from 2015 to 2021. *Remote Sensing* 15. URL: <https://www.mdpi.com/2072-4292/15/2/521>, doi:10.3390/rs15020521.

Wagner, F.H., Dalagnol, R., Sánchez, A.H., Hirye, M.C.M., Favrichon, S., Lee, J.H., Mauceri, S., Yang, Y., Saatchi, S., 2022. K-textures, a self supervised hard clustering deep learning algorithm for satellite images segmentation. URL: <https://arxiv.org/abs/2205.08671>, doi:10.48550/ARXIV.2205.08671.

Wagner, F.H., Roberts, S., Ritz, A.L., Carter, G., Dalagnol, R., Favrichon, S., Hirye, M.C., Brandt, M., Ciais, P., Saatchi, S., 2024. Sub-meter tree height mapping of California using aerial images and lidar-informed u-net model. *Remote Sensing of Environment* 305, 114099. URL: <https://www.sciencedirect.com/science/article/pii/S003442572400110X>, doi:<https://doi.org/10.1016/j.rse.2024.114099>.

Winstanley, P., Dalagnol, R., Mendiratta, S., Braga, D., Galvão, L.S., Bispo, P.d.C., 2024. Post-logging canopy gap dynamics and forest regeneration assessed using airborne lidar time series in the Brazilian Amazon with attribution to gap types and origins. *Remote Sensing* 16. URL: <https://www.mdpi.com/2072-4292/16/13/2319>, doi:10.3390/rs16132319.

Zapata-Ríos, G., Andreazza, C.S., Carnaval, A.C., da Costa Doria, C.R., Duponchelle, F., Flecker, A., Guayasamín, J.M., Heilpern, S., Jenkins, C.N., Maldonado, C., et al., 2022. Biological diversity and ecological networks in the Amazon. Chapter 3 URL: <https://www.theamazonwewant.org/amazon-assessment-report-2021/>.